MOX-Report No. 50/2018

The INTERNODES method for non-conforming discretizations of PDEs

Gervasio, P.; Quarteroni, A.

MOX, Dipartimento di Matematica
Politecnico di Milano, Via Bonardi 9 - 20133 Milano (Italy)

mox-dmat@polimi.it http://mox.polimi.it

The INTERNODES method for non-conforming discretizations of PDEs[1]

Paola Gervasio[2] and Alfio Quarteroni[3]

October 9, 2018

This paper is in memory of Professor Ben-Yu Guo

Abstract

INTERNODES is a general purpose method to deal with non-conforming discretizations of partial differential equations on regions partitioned into two or several disjoint subdomains. It exploits two intergrid interpolation operators, one for transfering the Dirichlet trace across the interfaces, the others for the Neumann trace. In this paper, in every subdomain the original problem is discretized by either the finite element method (FEM) or the spectral element method (SEM or *hp*-fem), using a priori non-matching grids and piece-wise polynomials of different degree. Other discretization methods however can be used. INTERNODES can also be applied to heterogeneous or multiphysics problems, that is problems that feature different differential operators inside adjacent subdomains. For instance, in this paper we apply the INTERNODES method to a Stokes-Darcy coupled problem that models the filtration of fluids in porous media. Our results highlight the flexibility of the method as well as its optimal rate of convergence with respect to the grid size and the polynomial degree.

Keywords. domain decomposition, non-conforming approximation, non-conforming grids, interpolation, finite element method, $hp-$finite element method, spectral element method

Contents

[1]Submitted

[2]DICATAM, Università degli Studi di Brescia, Brescia (Italy), paola.gervasio@unibs.it

[3]MOX, Department of Mathematics, Politecnico di Milano, Milano (Italy) and Institute of Mathematics, École Polytechnique Fédérale de Lausanne (EPFL), Lausanne (Switzerland) (honorary professor), alfio.quarteroni@polimi.it

1 Introduction

The INTERNODES method represents a numerical strategy to treat boundary value problems that are set on domains split in two (or several) subdomains with non-conforming discretizations. By that we mean that the grids used in each subdomain might not be the same at the interface separating the subdomains, or that finite dimensional approximation subspaces used in the different subdomains may not be the same.

INTERNODES was introduced in [5] for elliptic boundary value problems. Its theoretical analysis is carried out in [11]. The method uses two interpolation operators at the interface, one to transfer Dirichlet data from one domain to the adjacent domain, the other to transfer Neumann data in the opposite direction. Its numerical realization is very simple, it only involves rectangular matrices whose entries depend only on the node locations, plus two interface mass matrices that are defined independently from each side, without any cross coupling of the shape functions belonging to different subdomains.

In this paper we will review the INTERNODES method and discuss several issues concerning its practical implementation, the mathematical setting for the case of multiple subdomains sharing common cross-points, the efficient solution of the associated linear algebraic system, in the context of an elliptic boundary value-problems and of the coupled Stokes-Darcy problem. Several numerical tests are carried out in order to provide clear evidence to the theoretical properties of INTERNODES.

INTERNODES is an alternative to projection-based methods like mortar [2], or other interpolation-based method like GFEM/XFEM [15]. Differently than in mortar methods, no cross-mass matrix involving basis functions living on different grids of the interface are required by INTERNODES to build the intergrid operators. Instead, two separate interface mass matrices (separately on either interface) are used. The substantial difference between GFEM/XFEM methods and INTERNODES consists in the fact that the former ones use a partition of unity to enrich the finite element space, while the latter does not add any shape function to those of the local finite element subspaces.

Its great generality and flexibility makes INTERNODES suitable also to address heterogeneous (multiphysics) problems, that is the coupling between different kind of partial differential equations set on the different subdomains.

As an abstract instance of heterogeneous problem we consider the following one (we assume for the sake of exposition that Ω is split into only two subdomains): given a function f defined in Ω, we look for u_1 in Ω_1 and u_2 in Ω_2 such that

$$
\begin{aligned}
&L_k(u_k) = f && \text{in } \Omega_k, \quad k = 1, 2, && (1)\\
&\Phi_2(u_2) = \Phi_1(u_1) && \text{on } \Gamma \quad \text{(Dirichlet-like condition)}, && (2)\\
&\Psi_1(u_1) + \Psi_2(u_2) = 0 && \text{on } \Gamma \quad \text{(Neumann-like condition)}, && (3)\\
&\text{boundary conditions} && \text{on } \partial\Omega, && (4)
\end{aligned}
$$

where L_1 and L_2 are two differential operators while, for $k = 1, 2$, Φ_k and Ψ_k are suitable boundary operators restricted to the interface Γ, that depend upon the nature of the differential operators L_1 and L_2. More specifically, Neumann conditions refer here to natural conditions that are enforced *weakly*, whereas Dirichlet conditions identify those *essential* conditions that are enforced directly in the solution subspaces, via a suitable choice of trial functions (see, e.g., [21]). Typically for second order differential operators there is one Dirichlet-like condition and one Neumann-like condition, however more general situations are admissible.

In this regard, an application of INTERNODES to fluid-structure interaction problems is addressed in [10] and [7], whereas in [12] the method is applied to the numerical solution of a Stokes-Darcy problem for the coupling of surface and subsurface flow fields.

2 INTERNODES for Elliptic Problems

Let $\Omega \subset \mathbb{R}^d$, with $d = 2,\ 3$, be an open domain with Lipschitz boundary $\partial\Omega$. $\partial\Omega_N$ and $\partial\Omega_D$ are suitable disjoint subsets of $\partial\Omega$ such that $\overline{\partial\Omega_D} \cup \overline{\partial\Omega_N} = \partial\Omega$. We make the following assumptions.

Given the functions f defined in Ω, g_D defined on Γ_D and g_N on Γ_N, we look for the solution u of the second order elliptic problem

$$
\begin{cases}
Lu = f & \text{in } \Omega,\\
u = g_D & \text{on } \partial\Omega_D,\\
\partial_L u = g_N & \text{on } \partial\Omega_N,
\end{cases}
\tag{5}
$$

where $\partial_L u$ is the conormal derivative associated with the differential operator L on $\partial\Omega$.

After setting

$$V = H^1_{\partial\Omega_D}(\Omega) = \{v \in H^1(\Omega) : \ v = 0 \text{ on } \partial\Omega_D\}, \tag{6}$$

the weak form of problem (5) reads: find $u \in H^1(\Omega)$ with $u = g_D$ on $\partial\Omega_D$ such that

$$a(u, v) = \mathcal{F}(v) \qquad \forall v \in V, \tag{7}$$

where $a : V \times V \to \mathbb{R}$ is the bilinear form associated with the differential operator L, $\mathcal{F} : V \to \mathbb{R}$ is the linear functional

$$\mathcal{F}(v) = (f, v)_{L^2(\Omega)} + \langle g_N, v\rangle_{\partial\Omega_N},$$

while $(\cdot,\cdot)_{L^2(\Omega)}$ and $\langle\cdot,\cdot\rangle_{\partial\Omega_N}$ denote the inner product in $L^2(\Omega)$ and the duality pairing between $H^{1/2}(\partial\Omega_N)$ and $H^{-1/2}(\partial\Omega_N)$, respectively.

For instance, if

$$Lu = -\nabla\cdot(\alpha\nabla u) + \gamma u, \tag{8}$$

with α and γ two suitable functions defined in Ω, then

$$a(u, v) = \int_\Omega (\alpha\nabla u\cdot\nabla v + \gamma uv)d\Omega, \quad \forall u, v \in H^1(\Omega). \tag{9}$$

Provided that the bilinear form a is continuous and coercive in V and that the data are sufficiently regular so that $\mathcal{F}$ is continuous on V, there exists a unique solution of (7) that is stable w.r.t. f, g_D and g_N (see, e.g., [22]).

We partition Ω into two non-overlapping subdomains Ω_1 and Ω_2 with Lipschitz boundary and such that $\overline{\Omega} = \overline{\Omega_1 \cup \Omega_2}$. $\Gamma(= \overline{\Gamma}) = \partial\Omega_1 \cap \partial\Omega_2$ is the common interface and, for $k = 1, 2$, we set $\partial\Omega_{D,k} = \partial\Omega_D \cap \partial\Omega_k$ and $\partial\Omega_{N,k} = \partial\Omega_N \cap \partial\Omega_k$.

For $k = 1, 2$ let us introduce the local spaces

$$V_k = \{v \in H^1(\Omega_k) \mid v = 0 \text{ on } \partial\Omega_{D,k}\}, \quad V_k^0 = \{v \in V_k \mid v = 0 \text{ on } \Gamma\}, \tag{10}$$

let a_k and $\mathcal{F}_k$ denote the restriction of the bilinear form a and of the linear functional $\mathcal{F}$ to Ω_k, respectively, and let Λ be the space of traces of the elements of V on the interface Γ:

$$\Lambda = \{\lambda \in H^{1/2}(\Gamma) : \ \exists v \in V : v|_\Gamma = \lambda\}. \tag{11}$$

For $k = 1, 2$, let u_k be the restriction of the solution u of (7) to Ω_k, then u_1 and u_2 are the solution of the *transmission problem* (see [4, Ch. VII, Sect. 4])

$$\begin{cases} Lu_k = f & \text{in } \Omega_k, \quad k = 1, 2, \\ u_1 = u_2, & \text{on } \Gamma, \\ \partial_{L_1} u_1 + \partial_{L_2} u_2 = 0 & \text{on } \Gamma, \\ u_k = g_D & \text{on } \partial\Omega_{D,k}, \\ \partial_{L_k} u_k = g_N & \text{on } \partial\Omega_{N,k}, \end{cases} \tag{12}$$

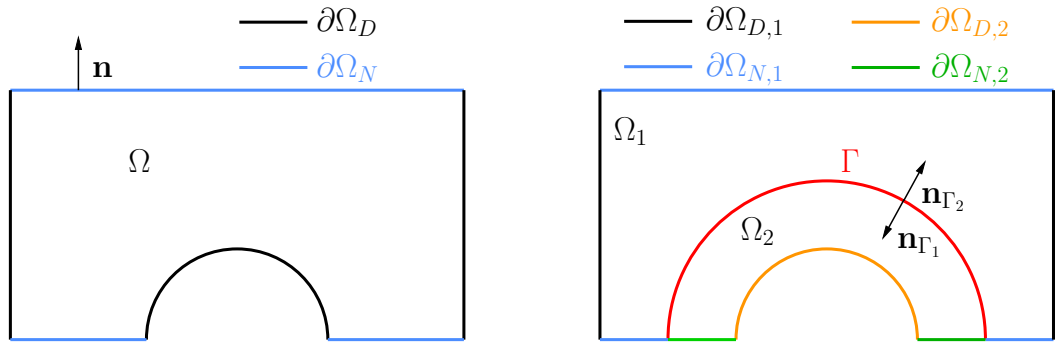

Figure 1: The computational domain Ω (at left) and its decomposition into two subdomains Ω_1 and Ω_2 with sharp interface Γ

where $\partial_{L_k} u_k$ denotes the *conormal derivative* associated with the differential operator L in Ω_k. For instance, when L is as in (8), the conormal derivative is

$$\partial_{L_k} u_k = \alpha_k \frac{\partial u_k}{\partial \mathbf{n}_k}$$

where $\alpha_k = \alpha_{|\Omega_k}$ and $\mathbf{n}_k$ is the outward unit normal vector to $\partial\Omega_k$ (in particular on Γ, we have $\mathbf{n}_1 = -\mathbf{n}_2$ and we denote by $\mathbf{n}_{\Gamma_k}$ the restriction of $\mathbf{n}_k$ to Γ,[1] see Fig. 1).

The weak form of the transmission problem (12) reads (see [23, Lemma 1.2.1]): for $k = 1, 2$ find $u_k \in H^1(\Omega_k)$ with $u_k|_{\partial\Omega_{D,k}} = g_D$ such that

$$\begin{cases} a_k(u_k, v_k^0) = \mathcal{F}_k(v_k^0) & \forall v_k^0 \in V_k^0, \quad k = 1, 2 \\ u_2 = u_1 & \text{on } \Gamma, \\ \displaystyle\sum_{k=1,2} a_k(u_k, \mathcal{R}_k\eta) = \sum_{k=1,2} \mathcal{F}_k(\mathcal{R}_k\eta) & \forall \eta \in \Lambda, \end{cases} \tag{13}$$

where

$$\mathcal{R}_k : \Lambda \to V_k, \quad s.t. \quad (\mathcal{R}_k\eta)|_\Gamma = \eta \qquad \forall \eta \in \Lambda \tag{14}$$

denotes any possible linear and continuous *lifting operator* from Γ to Ω_k.

Remark 1. *Let $\langle \cdot, \cdot \rangle_\Gamma$ denote the duality between Λ and its dual Λ'. If homogeneous boundary conditions (of either Dirichlet and Neumann type) are given on $\partial\Omega$, by counter-integration by parts, the interface equation $(13)_3$ is equivalent to*

$$\langle \partial_{L_1} u_1 + \partial_{L_2} u_2, \eta \rangle_\Gamma = 0 \qquad \forall \eta \in \Lambda, \tag{15}$$

and therefore to the transmission condition $(12)_3$.

Remark 2. *In the next Sections we present INTERNODES applied to the transmission problem (12) or, equivalently, to the weak form (13) provided that the bilinear form a*

[1] We assume that Γ is sufficiently regular to allow the conormal derivative of u to be well defined. This is certainly the case if Γ is of class $C^{1,1}$ (see [14, Def. 1.2.1.2]).

is continuous and coercive in V and the linear functional $\mathcal{F}$ is continuous in V. Nevertheless, we point out that INTERNODES can be applied to many other transmission problems arising, e.g., from Advection-Diffusion-Reaction equations, Linear Elasticity equations, Stokes equations, etc.

Before introducing INTERNODES, we briefly recall the discretization of the two-domains problem (13) by conforming methods.

2.1 Recall on conforming discretization in a domain decomposition framework

Let us consider a partition $\mathcal{T}_h = \cup_m T_m$ of the global domain Ω in either simplices (triangles if $d = 2$ or tetrahedra if $d = 3$) or quads (i.e. quadrilaterals if $d = 2$ or hexahedra if $d = 3$) depending on a positive parameter (the grid size) $h > 0$.

Following standard assumptions, if T_m are simplices, we require $\mathcal{T}_h$ to be affine, regular, and quasi-uniform (see [22, Ch. 3]), while if T_m are quads, we require that any T_m is the image through a C^1 diffeomorfism $\mathbf{F}_{T_m}$ of the reference quad $\hat{T} = [-1, 1]^d$ (see, e.g., [22]). Moreover, for any $T_m \in \mathcal{T}_h$, we assume that $\partial T_m \cap \partial\Omega$ fully belongs to either $\partial\Omega_D$ or $\partial\Omega_N$.

Let p be a positive integer. We shall denote by $\mathbb{P}_p$ the usual space of algebraic polynomials of total degree less than or equal to p, and by $\mathbb{Q}_p$ the usual space of algebraic polynomials of degree less than or equal to p with respect to each variable.

The finite (or spectral) element approximation space associated with $\mathcal{T}_h$ is

$$X_h^p = \{v \in C^0(\overline{\Omega}) : \ v_{|T_m} \in \mathcal{Q}_p, \ \forall T_m \in \mathcal{T}_h\} \tag{16}$$

where $\mathcal{Q}_p = \mathbb{P}_p$ in the simplicial case and $\mathcal{Q}_p = \mathbb{Q}_p \circ \mathbf{F}_{T_m}^{-1}$ for quads.

Then we define the finite dimensional space

$$V_h = \{v \in X_h^p : \ v = 0 \text{ on } \partial\Omega_D\} \tag{17}$$

and let $g_{D,h}$ be a suitable approximation of the boundary datum g_D (for example the interpolation of g_D on the space formed by the trace functions on $\partial\Omega_D$ of the functions in X_h^p).

The Galerkin finite element approximation of the monodomain weak problem (7) reads: find $u_h \in X_h^p$ with $u_h = g_{D,h}$ such that

$$a(u_h, v_h) = \mathcal{F}(v_h) \qquad \forall v_h \in V_h. \tag{18}$$

Now, let us consider the decomposition of Ω into the subdomains Ω_1 and Ω_2 as described above and assume that the triangulations $\mathcal{T}_h$ are such that Γ does not cut any element $T_m \in \mathcal{T}_h$. The triangulations $\mathcal{T}_{1,h}$ and $\mathcal{T}_{2,h}$ induced by $\mathcal{T}_h$ on Ω_1 and Ω_2 are therefore compatible on Γ, that is they share the same edges (if $d = 2$) or faces (if $d = 3$). See Fig. 2, right.

In each Ω_k $(k = 1, 2)$ we introduce the finite element approximation space

$$X_{k,h} = \{v \in C^0(\overline{\Omega}_k) \ : \ v_{|T_m} \in \mathcal{Q}_p, \ \forall T_m \in \mathcal{T}_{k,h}\}, \tag{19}$$

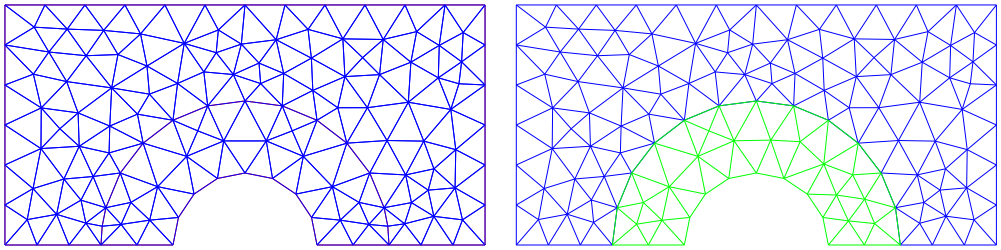

Figure 2: At left, the triangulation $\mathcal{T}_h$ in Ω. At right, the triangulations $\mathcal{T}_{1,h}$ (blue) in Ω_1 and $\mathcal{T}_{2,h}$ (green) in Ω_2 induced by $\mathcal{T}_h$. Notice that they are compatible on Γ

and the finite dimensional subspaces of V_k and V_k^0

$$V_{k,h} = X_{k,h} \cap V_k, \qquad V_{k,h}^0 = X_{k,h} \cap V_k^0. \tag{20}$$

Moreover, we consider the space of finite dimensional traces on Γ

$$Y_h = \{\lambda = v|_\Gamma,\ v \in X_{1,h} \cup X_{2,h}\}, \qquad \Lambda_h = \{\lambda = v|_\Gamma,\ v \in V_{1,h} \cup V_{2,h}\} \subset \Lambda. \tag{21}$$

Remark 3. *Notice that $X_{k,h}$, $V_{k,h}$, $V_{k,h}^0$, Y_h and Λ_h depend also on the local polynomial degree p, nevertheless this dependence is understood.*

For $k = 1, 2$ we define the linear and continuous *discrete lifting operators*

$$\mathcal{R}_{k,h} : \Lambda_h \to V_{k,h}, \quad s.t. \quad (\mathcal{R}_{k,h}\eta_h)|_\Gamma = \eta_h, \quad \forall \eta_h \in \Lambda_h. \tag{22}$$

In practical implementation, $\mathcal{R}_{k,h_k}\eta_h$ can be chosen as the *finite element interpolant* that matches the values of η_h at the finite element nodes on Γ and the zero values at any other finite element node of $\mathcal{T}_{k,h} \setminus \Gamma$.

The discrete weak form of the transmission problem (18) reads: for $k = 1, 2$ find $u_{k,h} \in X_{k,h}$ such that $u_{k,h} = g_{D,h}$ on $\partial\Omega_{D,k}$ such that

$$\begin{cases} a_k(u_{k,h}, v_{k,h}^0) = \mathcal{F}_k(v_{k,h}^0) & \forall v_{k,h}^0 \in V_{k,h}^0,\ k = 1, 2 \\ u_{2,h} = u_{1,h} & \text{on } \Gamma, \\ \displaystyle\sum_{k=1,2} a_k(u_{k,h}, \mathcal{R}_{k,h}\eta_h) = \sum_{k=1,2} \mathcal{F}_k(\mathcal{R}_{k,h}\eta_h) & \forall \eta_h \in \Lambda_h. \end{cases} \tag{23}$$

Problem (23) is actually equivalent to (18), in the sense that $u_{k,h} = u_{h|\Omega_k}$, for $k = 1, 2$ (see [23, Sect. 2.1]).

Defining the *discrete residual functionals* $r_{k,h}$ by the relations

$$\langle r_{k,h}, \eta_h \rangle_\Gamma = a_k(u_{k,h}, \mathcal{R}_{k,h}\eta_h) - \mathcal{F}_k(\mathcal{R}_{k,h}\eta_h) \quad \text{for any } \eta_h \in \Lambda_h, \tag{24}$$

the interface equation $(23)_3$ is equivalent to

$$\langle r_{1,h} + r_{2,h}, \eta_h \rangle_\Gamma = 0 \quad \text{for any } \eta_h \in \Lambda_h. \tag{25}$$

The finite dimensional functionals $r_{k,h}$ represent the approximations of the distributional derivatives $\partial_{L_k} u_k$ on Γ. Then (25) can be regarded as the discrete counterpart of (15).

2.2 Non-conforming discretization

Now we consider two a-priori *independent families of triangulations* $\mathcal{T}_{1,h_1}$ in Ω_1 and $\mathcal{T}_{2,h_2}$ in Ω_2, respectively. This means that the meshes in Ω_1 and in Ω_2 can be non-conforming on Γ and characterized by different mesh-sizes h_1 and h_2. Moreover, different polynomial degrees p_1 and p_2 can be used to define the finite element spaces. Inside each subdomain Ω_k we assume that the triangulations $\mathcal{T}_{k,h_k}$ are affine, regular and quasi-uniform if T_m are simplices, while we require that any T_m is the image through a C^1 diffeomorfism $\mathbf{F}_{T_m}$ of the reference quad $\hat{T} = [-1,1]^d$ if T_m are quads (see, e.g., [22]).

From now on, the finite element approximation spaces are (for $k = 1, 2$):

$$\begin{aligned} &X_{k,h_k} = \{v \in C^0(\overline{\Omega}_k) \,:\, v_{|T_m} \in \mathcal{Q}_{p_k},\ \forall T_m \in \mathcal{T}_{k,h_k}\}, \\ &V_{k,h_k} = X_{k,h_k} \cap V_k, \qquad V^0_{k,h_k} = \{v \in V_{k,h_k}, v|_\Gamma = 0\}, \end{aligned} \tag{26}$$

(where $\mathcal{Q}_{p_k} = \mathbb{P}_{p_k}$ if the T_m are simplices and $\mathcal{Q}_{p_k} = \mathbb{Q}_{p_k} \circ \mathbf{F}^{-1}_{T_m}$ if the T_m are quads) while the spaces of traces on Γ are

$$Y_{k,h_k} = \{\lambda = v|_\Gamma,\ v \in X_{k,h_k}\} \text{ and } \Lambda_{k,h_k} = \{\lambda = v|_\Gamma,\ v \in V_{k,h_k}\}. \tag{27}$$

We set $\overline{N}_k = \dim(X_{k,h_k})$, $N_k = \dim(V_{k,h_k})$, $N^0_k = \dim(V^0_{k,h_k})$, $\overline{n}_k = \dim(Y_{k,h_k})$, and $n_k = \dim(\Lambda_{k,h_k})$.

The space Λ_{k,h_k} takes into account the essential boundary conditions, while Y_{k,h_k} does not. Thus, if $\partial\Omega \cap \partial\Gamma \subset \partial\Omega_N$, then $\Lambda_{k,h_k} = Y_{k,h_k}$ and $n_k = \overline{n}_k$, otherwise $n_k < \overline{n}_k$ because the degrees of freedom associated with the nodes in $\partial\Omega_D \cap \partial\Gamma$ are eliminated.

The Lagrange basis functions of V_{k,h_k} (for $k = 1, 2$) associated with the nodes $\mathbf{x}^{(k)}_i$ of the mesh $\mathcal{T}_{k,h_k}$ are denoted by $\{\varphi^{(k)}_i\}$ for $i = 1, \ldots, N_k$.

We denote by Γ_1 and Γ_2 the internal boundaries of Ω_1 and Ω_2, respectively, induced by the triangulations $\mathcal{T}_{1,h_1}$ and $\mathcal{T}_{2,h_2}$. If Γ is a straight segment, then $\Gamma_1 = \Gamma_2 = \Gamma$, otherwise Γ_1 and Γ_2 can be different (see Fig. 4).

For $k = 1, 2$, let $\{\mathbf{x}^{(\Gamma_k)}_1, \ldots, \mathbf{x}^{(\Gamma_k)}_{\overline{n}_k}\} \in \Gamma_k (= \overline{\Gamma}_k)$ be the nodes induced by the mesh $\mathcal{T}_{k,h_k}$.

The Lagrange basis functions of Y_{k,h_k} are denoted by $\{\mu^{(k)}_i\}$ for $i = 1, \ldots, \overline{n}_k$.

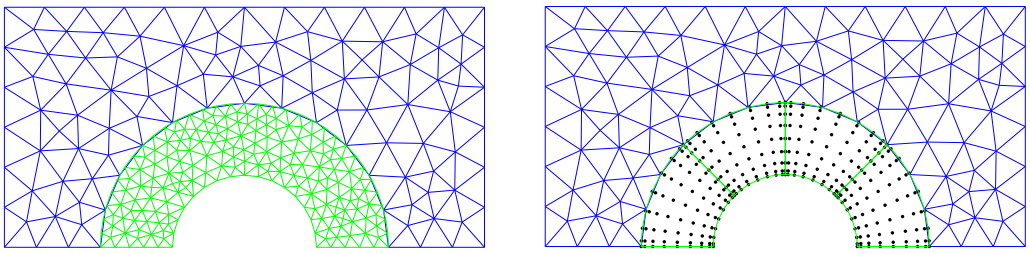

Figure 3: The triangulations $\mathcal{T}_{1,h}$ (blue) and $\mathcal{T}_{2,h}$ (green) are non-conforming on Γ. At left, FEM-FEM coupling. At right, FEM-SEM coupling

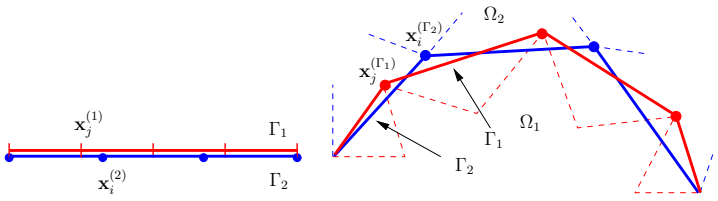

Figure 4: Γ_1 and Γ_2 induced by the triangulations $\mathcal{T}_{1,h_1}$ and $\mathcal{T}_{2,h_2}$

In formulating the INTERNODES method we will make use of the *interface mass matrices* M_{Γ_k}:

$$(M_{\Gamma_k})_{ij} = (\mu_j^{(k)}, \mu_i^{(k)})_{L^2(\Gamma_k)}, \qquad i,j = 1,\ldots,\overline{n}_k, \quad k = 1,2. \tag{28}$$

We will also need the canonical *dual basis* $\{\Phi_i^{(k)}\}_{i=1}^{\overline{n}_k}$ of Y'_{k,h_k} (the dual space of Y_{k,h_k}) defined by

$$\langle \Phi_i^{(k)}, \mu_j^{(k)} \rangle = (\Phi_i^{(k)}, \mu_j^{(k)})_{L^2(\Gamma_k)} = \delta_{ij}, \quad i,j = 1,\ldots,\overline{n}_k. \tag{29}$$

It holds that (see, e.g., [3])

$$\Phi_i^{(k)} = \sum_{j=1}^{\overline{n}_k} (M_{\Gamma_k}^{-1})_{ji} \mu_j^{(k)}, \qquad i = 1,\ldots,\overline{n}_k, \tag{30}$$

meaning that Y'_{k,h_k} and Y_{k,h_k} are in fact the same (finite dimensional) linear space.

By expanding any element $r_{k,h_k} \in Y'_{k,h_k}$ with respect to the dual basis

$$r_{k,h_k}(\mathbf{x}) = \sum_{i=1}^{\overline{n}_k} r_i^{(k)} \Phi_i^{(k)}(\mathbf{x}) \qquad \forall \mathbf{x} \in \Gamma_k,$$

we note that, thanks to (30),

$$r_{k,h_k}(\mathbf{x}) = \sum_{j=1}^{\overline{n}_k} \underbrace{\left(\sum_{i=1}^{\overline{n}_k} (M_{\Gamma_k}^{-1})_{ji} r_i^{(k)} \right)}_{z_j^{(k)}} \mu_j^{(k)}(\mathbf{x}) = \sum_{j=1}^{\overline{n}_k} z_j^{(k)} \mu_j^{(k)}(\mathbf{x}) \qquad \forall \mathbf{x} \in \Gamma_k, \tag{31}$$

hence, (31) provides the expansion of r_{k,h_k} with respect to the Lagrange basis $\{\mu_i^{(k)}\}$.

Denoting by $\mathbf{z}_{\overline{\Gamma}_k}$, $\mathbf{r}_{\overline{\Gamma}_k} \in \mathbb{R}^{\overline{n}_k}$ the vectors whose entries are the values $z_j^{(k)}$ and $r_i^{(k)}$, respectively, it holds

$$\mathbf{z}_{\overline{\Gamma}_k} = M_{\Gamma_k}^{-1} \mathbf{r}_{\overline{\Gamma}_k}. \tag{32}$$

The interface mass matrix M_{Γ_k} and its inverse play the role of transfer matrices from the Lagrange basis to the dual one and viceversa, respectively.

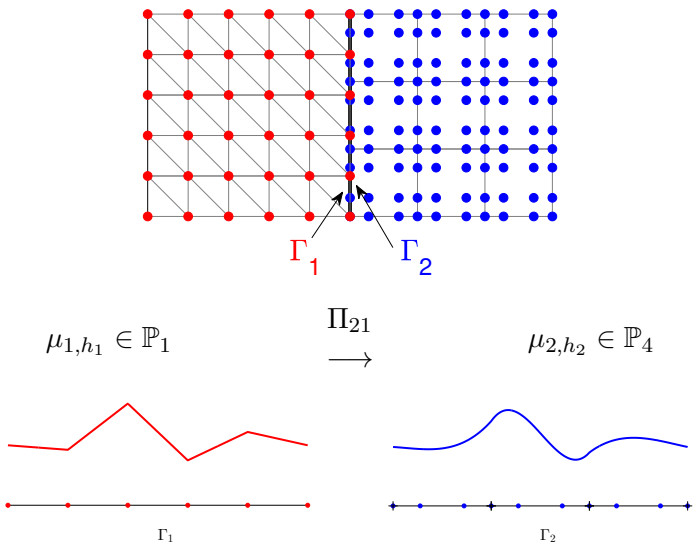

Figure 5: The interpolation from Γ_1 to Γ_2

2.2.1 Interpolation and intergrid operators

We introduce two independent operators that exchange information between the two independent grids on the interface Γ:

$$\Pi_{12} : Y_{2,h_2} \to Y_{1,h_1}, \quad \text{and} \quad \Pi_{21} : Y_{1,h_1} \to Y_{2,h_2}.$$

When Γ_1 and Γ_2 coincide (e.g. this is the case of straigth interface Γ as in Fig. 4, left), then Π_{12} and Π_{21} are the classical Lagrange interpolation operators defined by the relations (see Fig. 5):

$$(\Pi_{12}\mu_{2,h_2})(\mathbf{x}_i^{(\Gamma_1)}) = \mu_{2,h_2}(\mathbf{x}_i^{(\Gamma_1)}), \quad i = 1, \ldots, \overline{n}_1, \qquad \forall \mu_{2,h_2} \in Y_{2,h_2}, \tag{33}$$

$$(\Pi_{21}\mu_{1,h_1})(\mathbf{x}_i^{(\Gamma_2)}) = \mu_{1,h_1}(\mathbf{x}_i^{(\Gamma_2)}), \quad i = 1, \ldots, \overline{n}_2, \qquad \forall \mu_{1,h_1} \in Y_{1,h_1}. \tag{34}$$

The (rectangular) matrices associated with Π_{12} and Π_{21} are, respectively, $R_{12} \in \mathbb{R}^{\overline{n}_1 \times \overline{n}_2}$ and $R_{21} \in \mathbb{R}^{\overline{n}_2 \times \overline{n}_1}$ and they are defined by

$$\begin{aligned} (R_{12})_{ij} &= (\Pi_{12}\mu_j^{(2)})(\mathbf{x}_i^{(\Gamma_1)}) \qquad i = 1, \ldots, \overline{n}_1, \ j = 1, \ldots, \overline{n}_2, \\ (R_{21})_{ij} &= (\Pi_{21}\mu_j^{(1)})(\mathbf{x}_i^{(\Gamma_2)}) \qquad i = 1, \ldots, \overline{n}_2, \ j = 1, \ldots, \overline{n}_1, \end{aligned} \tag{35}$$

where $\{\mu_i^{(k)}\}$ are the Lagrange basis functions of Y_{k,h_k}, for $k = 1, 2$ and $i = 1, \ldots, \overline{n}_k$.

Obviously, in the conforming case for which $\Gamma_1 = \Gamma_2$, $h_1 = h_2$ and $p_1 = p_2$, the interpolation operators Π_{12} and Π_{21} are the identity operator and $R_{12} = R_{21} = I$ (the identity matrix of size $\overline{n}_1 = \overline{n}_2$).

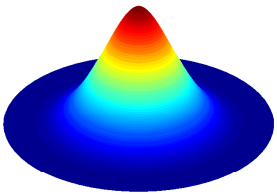

Figure 6: An example of locally supported C^2- Wendland radial basis function $\tilde{\phi}_i^{(k)}(\mathbf{x})$

2.2.2 Interpolation for non-conforming interfaces

When Γ_1 and Γ_2 are geometrical non-conforming (as in the right picture of Fig. 4), we define Π_{12} and Π_{21} as the Rescaled Localized Radial Basis Function (RL-RBF) interpolation operators introduced in formula (3.1) of [6].

More precisely, for $i = 1, \ldots, \overline{n}_k$ let

$$\tilde{\phi}_i^{(k)}(\mathbf{x}) = \phi(\|\mathbf{x} - \mathbf{x}_i^{(\Gamma_k)}\|, r) = \max\left\{0, \left(1 - \frac{\|\mathbf{x} - \mathbf{x}_i^{(\Gamma_k)}\|}{r}\right)^4\right\}\left(1 + 4\frac{\|\mathbf{x} - \mathbf{x}_i^{(\Gamma_k)}\|}{r}\right)$$

be the locally supported C^2- Wendland radial basis function [25] centered at $\mathbf{x}_i^{(\Gamma_k)}$ with radius $r > 0$ (see Fig. 6).

For any continuous function f defined in Ω, the Radial Basis Function (RBF) interpolant of f at the nodes $\mathbf{x}_i^{(\Gamma_k)}$ (for $i = 1, \ldots, \overline{n}_k$ and for any $k = 1, 2$) reads

$$(\Pi_{RBF}^{(k)} f)(\mathbf{x}) = \sum_{i=1}^{\overline{n}_k} (\gamma_f^{(k)})_i \tilde{\phi}_i^{(k)}(\mathbf{x}),$$

where the real values $(\gamma_f^{(k)})_i$ are the solutions of the linear system

$$(\Pi_{RBF}^{(k)} f)(\mathbf{x}_j^{(\Gamma_k)}) = \sum_{i=1}^{\overline{n}_k} (\gamma_f^{(k)})_i \tilde{\phi}_i^{(k)}(\mathbf{x}_j^{(\Gamma_k)}) = f(\mathbf{x}_j^{(\Gamma_k)}), \qquad j = 1, \ldots, \overline{n}_k.$$

After setting $g(x) \equiv 1$, the RL-RBF interpolant of f at the nodes $\mathbf{x}_i^{(\Gamma_k)}$ reads ([6]):

$$(\Pi_{RL-RBF}^{(k)} f)(\mathbf{x}) = \frac{(\Pi_{RBF}^{(k)} f)(\mathbf{x})}{(\Pi_{RBF}^{(k)} g)(\mathbf{x})} = \frac{\sum_{i=1}^{\overline{n}_k} (\gamma_f^{(k)})_i \tilde{\phi}_i^{(k)}(\mathbf{x})}{\sum_{i=1}^{\overline{n}_k} (\gamma_g^{(k)})_i \tilde{\phi}_i^{(k)}(\mathbf{x})}. \tag{36}$$

Then we define the interpolation operators $\Pi_{12} : Y_{2,h_2} \to Y_{1,h_1}$ and $\Pi_{21} : Y_{1,h_1} \to Y_{2,h_2}$ such that for any $\mu_{2,h_2} \in Y_{2,h_2}$ and $\mu_{1,h_1} \in Y_{1,h_1}$,

$$\begin{aligned} (\Pi_{12}\mu_{2,h_2})(\mathbf{x}_j^{(\Gamma_1)}) &= (\Pi_{RL-RBF}^{(2)}\mu_{2,h_2})(\mathbf{x}_j^{(\Gamma_1)}) \quad j = 1, \ldots, \overline{n}_1, \\ (\Pi_{21}\mu_{1,h_1})(\mathbf{x}_j^{(\Gamma_2)}) &= (\Pi_{RL-RBF}^{(1)}\mu_{1,h_1})(\mathbf{x}_j^{(\Gamma_2)}) \quad j = 1, \ldots, \overline{n}_2. \end{aligned} \tag{37}$$

The (rectangular) matrices associated with the RL-RBF interpolation operators (37) are defined as in (35). More precisely, if we set

$$(\Phi_{k\ell})_{ij} = \tilde{\phi}_j^{(\ell)}(\mathbf{x}_i^{(\Gamma_k)}) \quad \text{for } k,\ell \in \{1,2\},\ i = 1,\dots,\overline{n}_k,\ j = 1,\dots,\overline{n}_\ell,$$

we have

$$\begin{aligned}
(R_{21})_{ij} &= (\Pi_{21}\mu_j^{(1)})(\mathbf{x}_i^{(\Gamma_2)}) = \frac{(\Phi_{21}\Phi_{11}^{-1})_{ij}}{(\Phi_{21}\Phi_{11}^{-1}\mathbf{1})_i}, \qquad i = 1,\dots,\overline{n}_2,\ j = 1,\dots,\overline{n}_1,\\
(R_{12})_{ij} &= (\Pi_{12}\mu_j^{(2)})(\mathbf{x}_i^{(\Gamma_1)}) = \frac{(\Phi_{12}\Phi_{22}^{-1})_{ij}}{(\Phi_{12}\Phi_{22}^{-1}\mathbf{1})_i}, \qquad i = 1,\dots,\overline{n}_1,\ j = 1,\dots,\overline{n}_2,
\end{aligned} \tag{38}$$

where $\mathbf{1}$ is the column array with all the entries equal to 1 and $\{\mu_i^{(k)}\}$ are the Lagrange basis functions of Y_{k,h_k}.

Remark 4. *We notice that only information associated with the interface nodes (more precisely, the nodes coordinates) are needed to assemble both the interface mass matrices and the interpolation matrices for both the Lagrange and the RL-RBF interpolation approaches.*

Remark 5. *Using only one intergrid interpolation operator would not guarantee an accurate non-conforming method; this would yield the so-called* pointwise matching *discussed, e.g., in [2, 1], where both trial and test functions satisfy the relation* $v_{|\Gamma_2} = \Pi_{21} v_{|\Gamma_1}$. *In our approach, the second operator (*Π_{12} *that maps* Y_{2,h_2} *on* Y_{1,h_1}*) matches, in a suitable way, the fluxes across the interface.*

2.3 Formulation of INTERNODES

For $k = 1, 2$ we define two discrete linear and continuous *lifting operators*

$$\overline{\mathcal{R}}_k = \overline{\mathcal{R}}_{k,h_k} : Y_{k,h_k} \to X_{k,h_k}, \qquad s.t. \qquad (\overline{\mathcal{R}}_k \lambda_{k,h_k})|_{\Gamma_k} = \lambda_{k,h_k}, \tag{39}$$

such that, when restricted to Λ_{k,h_k}, $\overline{\mathcal{R}}_k$ coincides with the lifting $\mathcal{R}_{k,h_k}$ introduced in (22).

In practical implementation, we can define $\overline{\mathcal{R}}_k \lambda_{k,h_k}$ as the finite element interpolant that extends any $\lambda_{k,h_k} \in Y_{k,h_k}$ by setting to zero the values of $\overline{\mathcal{R}}_k \lambda_{k,h_k}$ at all nodes of $\mathcal{T}_{k,h_k}$ not belonging to Γ_k. In particular, if $\lambda_{k,h_k} = \mu_j^{(k)}$ (the jth Lagrange basis function on Γ_k), then $\overline{\mathcal{R}}_k \mu_j^{(k)}$ is the Lagrange basis function of X_{k,h_k} whose restriction on Γ_k coincides with $\mu_j^{(k)}$.

To start, let us consider the case when $\partial\Gamma \cap \partial\Omega_D = \emptyset$ (as, e.g., the situation of Fig. 1).

For any $u_{k,h_k} \in X_{k,h_k}$ and for any $k = 1, 2$ we define the scalar quantities:

$$(r_u^{(k)})_i = a_k(u_{k,h_k}, \overline{\mathcal{R}}_k \mu_i^{(k)}) - \mathcal{F}_k(\overline{\mathcal{R}}_k \mu_i^{(k)}) \quad i = 1,\dots,\overline{n}_k, \tag{40}$$

$$(z_u^{(k)})_j = \sum_{i=1}^{\overline{n}_k} (M_{\Gamma_k}^{-1})_{ji} (r_u^{(k)})_i, \qquad j = 1,\dots,\overline{n}_k, \tag{41}$$

and the functions

$$(r_u)_{k,h_k} = \sum_{j=1}^{\overline{n}_k} (z_u^{(k)})_j \mu_j^{(k)} \tag{42}$$

belonging to Y_{k,h_k}. (The subscript u highlights the dependence of r on u.)

Let g_{D,h_1} and g_{D,h_2} be two suitable approximations of the boundary datum g_D on $\partial\Omega_{D,1}$ and $\partial\Omega_{D,2}$, respectively.

The *weak form of INTERNODES* applied to (5) reads: find $u_{1,h_1} \in X_{1,h_1}$ with $u_{1,h_1} = g_{D,h_1}$ on $\partial\Omega_{D,1}$ and $u_{2,h_2} \in X_{2,h_2}$ with $u_{2,h_2} = g_{D,h_2}$ on $\partial\Omega_{D,2}$, such that

$$\begin{cases} a_k(u_{k,h_k}, v_{k,h_k}) = \mathcal{F}_k(v_{k,h_k}) & \forall v_{k,h_k} \in V^0_{k,h_k}, \quad k = 1,2 \\ u_{2,h_2} = \Pi_{21} u_{1,h_1} & \text{on } \Gamma_2, \\ (r_u)_{1,h_1} + \Pi_{12}(r_u)_{2,h_2} = 0 & \text{on } \Gamma_1. \end{cases} \tag{43}$$

(Notice that both the interpolations are made up to the boundary of the interfaces and not only at the internal nodes.)

For $k = 1, 2$, $(r_u)_{k,h_k} \in Y_{k,h_k}$ are the so-called *residuals* at the interface Γ_k and in fact they are the *discrete fluxes* across the interface, i.e. they represent the approximations of the conormal derivative $\partial_{L_k} u_k$ on Γ_k.

As a matter of fact, by counter integrating by parts (40) we have, for any $i = 1, \ldots, \overline{n}_k$,

$$\begin{aligned} (r_u^{(k)})_i &= a_k(u_{k,h_k}, \overline{\mathcal{R}}_k \mu_i^{(k)}) - \mathcal{F}_k(\overline{\mathcal{R}}_k \mu_i^{(k)}) \\ &= a_k(u_{k,h_k}, \overline{\mathcal{R}}_k \mu_i^{(k)}) - (f, \overline{\mathcal{R}}_k \mu_i^{(k)})_{L^2(\Omega_k)} - \langle g_N, \overline{\mathcal{R}}_k \mu_i^{(k)} \rangle_{\partial\Omega_{N,k}} \\ &= (Lu_{k,h_k}, \overline{\mathcal{R}}_k \mu_i^{(k)})_{L^2(\Omega_k)} - (f, \overline{\mathcal{R}}_k \mu_i^{(k)})_{L^2(\Omega_k)} - \langle g_N, \overline{\mathcal{R}}_k \mu_i^{(k)} \rangle_{\partial\Omega_{N,k}} \\ &\quad + \int_{\Gamma_k} \partial_{L_k} u_{k,h_k} \ \mu_i^{(k)} + \int_{\partial\Omega_{D,k}} \partial_{L_k} u_{k,h_k} \ \overline{\mathcal{R}}_k \mu_i^{(k)} + \int_{\partial\Omega_{N,k}} \partial_{L_k} u_{k,h_k} \ \overline{\mathcal{R}}_k \mu_i^{(k)} \\ &= \int_{\Gamma_k} \partial_{L_k} u_{k,h_k} \ \mu_i^{(k)} + \int_{\partial\Omega_{D,k}} \partial_{L_k} u_{k,h_k} \ \overline{\mathcal{R}}_k \mu_i^{(k)}. \end{aligned} \tag{44}$$

If, as usual in finite element context, $\overline{\mathcal{R}}_k \mu_i^{(k)}$ is taken as the finite element interpolant that extends $\mu_i^{(k)}$ to X_{k,h_k} and we assume that neither $\partial\Omega_{N,k}$ nor $\partial\Omega_{D,k}$ cut the edges of the elements in $\mathcal{T}_{k,h}$, then $\overline{\mathcal{R}}_k \mu_i^{(k)}|_{\partial\Omega_{D,k}}$ is null for any $i = 1, \ldots, \overline{n}_k$ (see Fig. 7, left, recalling that we are assuming $\partial\Gamma \cap \partial\Omega_D = \emptyset$) and it holds

$$(r_u^{(k)})_i = \int_{\Gamma_k} \partial_{L_k} u_{k,h_k} \ \mu_i^{(k)}, \qquad \text{for any } i = 1, \ldots, \overline{n}_k, \tag{45}$$

then $(r_u)_{k,h_k}$ is an approximation of the distributional derivative $\partial_{L_k} u_k$ on Γ_k.

When instead $\partial\Gamma \cap \partial\Omega_D \neq \emptyset$ (see Fig. 7, right), the lifting $\overline{\mathcal{R}}_k \mu_i^{(k)}$ may be non-null on $\partial\Omega_{D,k}$ (in particular it happens for the indices i associated with the nodes belonging

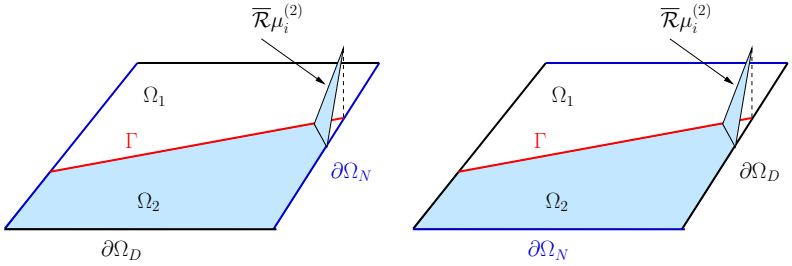

Figure 7: The liftings $\overline{\mathcal{R}}_k\mu_i^{(k)}$. At left, $\overline{\mathcal{R}}_k\mu_i^{(2)}|_{\partial\Omega_{D,2}} = 0$. At right $\overline{\mathcal{R}}_k\mu_i^{(2)}|_{\partial\Omega_{D,2}} \neq 0$

to $\Gamma_k \cap \partial\Omega_{D,k}$) and, in order to guarantee that (45) is satisfied, the definition (40) of $(r_u^{(k)})_i$ should be modified as follows (for any i s.t. $\mathbf{x}_i^{(\Gamma_k)} \in \Gamma_k \cap \partial\Omega_{D,k}$):

$$(r_u^{(k)})_i = a_k(u_{k,h_k}, \overline{\mathcal{R}}_k\mu_i^{(k)}) - \mathcal{F}_k(\overline{\mathcal{R}}_k\mu_i^{(k)}) - \int_{\partial\Omega_{D,k}} \partial_{L_k} u_{k,h_k}\ \overline{\mathcal{R}}_k\mu_i^{(k)}. \tag{46}$$

We notice that, when we consider conforming decompositions, the correction provided in (46) is not needed, thanks to the fact that the continuity of the fluxes is imposed only at the nodes internal to Γ, without invoking any interpolation process.

On the contrary, in the non-conforming case, it is mandatory to define correctly the residuals $(r_u)_{k,h_k}$ up to the boundary of Γ_k, since during the interpolation process (precisely through the operator Π_{12}) we act on all the degrees of freedom of Γ_2, included those on $\partial\Gamma_2$.

In conclusion, INTERNODES is defined by:

$$\begin{aligned} &(43) \text{ with } (40), (41), (42) \quad \text{if } \partial\Gamma \cap \partial\Omega_D = \emptyset, \\ &(43) \text{ with } (46), (41), (42) \quad \text{if } \partial\Gamma \cap \partial\Omega_D \neq \emptyset. \end{aligned}$$

We refer to Remark 9 for the implementation of the correction (46).

Remark 6. *The values $(r_u^{(k)})_i$ are not the coefficients of $(r_u)_{k,h_k}$ w.r.t. the Lagrange basis $\{\mu_i^{(k)}\}$ (on which we can apply the interpolation). Rather, they are the coefficients of $(r_u)_{k,h_k}$ w.r.t. the dual basis $\{\Phi_i^{(k)}\}_{i=1}^{\overline{n}_k}$ of Y'_{k,h_k} defined in (30). More precisely, it holds*

$$(r_u)_{k,h_k} = \sum_{i=1}^{\overline{n}_k} (r_u)_i^{(k)} \Phi_i^{(k)}.$$

Remark 7. *The domains Ω_1 and Ω_2 play differently in (43), more precisely the Dirichlet trace on Γ_1 is first interpolated and then transferred to Γ_2 (for this reason, mimicking the mortar notation, Ω_1 is named* master *subdomain and Ω_2* slave *subdomain).*

On the contrary, the Neumann trace on Γ_2, i.e. the residual, is first interpolated and then transferred to Γ_1.

Remark 8. *As previously pointed out, if the discretizations in Ω_1 and Ω_2 are conforming on Γ, then Π_{21} and Π_{12} are the identity operators, then problem (43) coincides with (23); (43) can therefore be regarded as the extension of (23) to the non-conforming case.*

2.4 Algebraic form of INTERNODES

Let us denote by $\{\varphi_i^{(k)}\}$, for $i = 1, \ldots, \overline{N}_k$, the Lagrange basis functions of $X_{k,h}^p$ associated with the nodes $\mathbf{x}_i$ of the mesh $\mathcal{T}_{k,h}$ and we define the following sets of indices:

$$\begin{array}{rcl} \mathcal{I}_{\overline{\Omega}_k} & = & \{1, \ldots, \overline{N}_k\}, \\ \mathcal{I}_k & = & \{i \in \mathcal{I}_{\overline{\Omega}_k} : \ \mathbf{x}_i \in \overline{\Omega}_k \setminus (\overline{\partial\Omega_{D,k}} \cup \mathring{\Gamma}_k)\}, \\ \mathcal{I}_{D_k} & = & \{i \in \mathcal{I}_{\overline{\Omega}_k} : \ \mathbf{x}_i \in \overline{\partial\Omega_{D,k}}\}, \\ \mathcal{I}_{\overline{\Gamma}_k} & = & \{i \in \mathcal{I}_{\overline{\Omega}_k} : \ \mathbf{x}_i \in \overline{\Gamma}_k\}, \\ \mathcal{I}_{\Gamma_k} & = & \{i \in \mathcal{I}_{\overline{\Omega}_k} : \ \mathbf{x}_i \in \overline{\Gamma}_k \setminus \overline{\partial\Omega_{D,k}}\}, \\ \mathcal{I}_{\Gamma_k^D} & = & \{i \in \mathcal{I}_{\overline{\Omega}_k} : \ \mathbf{x}_i \in \overline{\Gamma}_k \cap \overline{\partial\Omega_{D,k}}\}. \end{array} \tag{47}$$

Clearly, if $\partial\Gamma \cap \partial\Omega_D = \emptyset$, then $\mathcal{I}_{\overline{\Gamma}_k} = \mathcal{I}_{\Gamma_k}$ and $\mathcal{I}_{\Gamma_k^D} = \emptyset$.

As usual in finite element context, $\overline{\mathcal{R}}_k \mu_i^{(k)}$ is taken as the finite element interpolant that extends $\mu_i^{(k)}$ to X_{k,h_k}, thus there exists a unique $j = j(i) \in \mathcal{I}_{\overline{\Omega}_k}$ such that $\overline{\mathcal{R}}_k \mu_i^{(k)} = \varphi_j^{(k)}$.

For $k = 1, 2$, we define in a standard way the local stiffness matrices (see, e.g., [24, 23]), i.e.

$$A_{ij}^{(k)} = a_k(\varphi_j^{(k)}, \varphi_i^{(k)}), \quad i, j \in \mathcal{I}_{\overline{\Omega}_k},$$

then let

$$A_{kk} = A^{(k)}(\mathcal{I}_k, \mathcal{I}_k)$$

be the submatrix of $A^{(k)}$ obtained by taking both rows and columns of $A^{(k)}$ whose indices belong to $\mathcal{I}_k$. Similarly we define the submatrices $A_{\Gamma_k,\Gamma_k} = A^{(k)}(\mathcal{I}_{\Gamma_k}, \mathcal{I}_{\Gamma_k})$, $A_{\overline{\Gamma}_k,\overline{\Gamma}_k} = A^{(k)}(\mathcal{I}_{\overline{\Gamma}_k}, \mathcal{I}_{\overline{\Gamma}_k})$, $A_{k,\Gamma_k} = A^{(k)}(\mathcal{I}_k, \mathcal{I}_{\Gamma_k})$ and so on.

Moreover we define the arrays

$$\mathbf{f}^{(k)} = [\mathcal{F}_k(\varphi_i^{(k)})]_{i \in \mathcal{I}_{\overline{\Omega}_k}}, \quad \mathbf{u}^{(k)} = [u_{k,h_k}(\mathbf{x}_i^{(k)})]_{i \in \mathcal{I}_{\overline{\Omega}_k}}$$

and, by exploiting the same indexing notation as before, the subarrays

$$\begin{array}{lll} \mathbf{f}_k = \mathbf{f}^{(k)}(\mathcal{I}_k), & \mathbf{f}_{\overline{\Gamma}_k} = \mathbf{f}^{(k)}(\mathcal{I}_{\overline{\Gamma}_k}), & \mathbf{f}_{\Gamma_k} = \mathbf{f}^{(k)}(\mathcal{I}_{\Gamma_k}), \\ \mathbf{u}_k = \mathbf{u}^{(k)}(\mathcal{I}_k), & \mathbf{u}_{\overline{\Gamma}_k} = \mathbf{u}^{(k)}(\mathcal{I}_{\overline{\Gamma}_k}), & \mathbf{u}_{\Gamma_k} = \mathbf{u}^{(k)}(\mathcal{I}_{\Gamma_k}). \end{array}$$

Finally, we set

$$\begin{array}{ll} \mathbf{r}_{\Gamma_k} = [(r_u^{(k)})_i]_{i \in \mathcal{I}_{\Gamma_k}}, & \mathbf{r}_{\overline{\Gamma}_k} = [(r_u^{(k)})_i]_{i \in \mathcal{I}_{\overline{\Gamma}_k}}, \\ \mathbf{g}_{D_k} = [g_D(\mathbf{x}_i^{(k)})]_{i \in \mathcal{I}_{D_k}}, & \mathbf{g}_{\Gamma_k^D} = [g_D(\mathbf{x}_i^{(k)})]_{i \in \mathcal{I}_{\Gamma_k^D}}. \end{array}$$

In the case that $\mathcal{T}_{1,h_1}$ and $\mathcal{T}_{2,h_2}$ are conforming on Γ (in which case $h_1 = h_2$ and $\overline{n}_1 = \overline{n}_2$), the algebraic counterpart of the conforming 2-domains problem (23) reads

$$\begin{bmatrix} A_{1,1} & A_{1,\Gamma_1} & 0 \\ A_{\Gamma_1,1} & A_{\Gamma_1,\Gamma_1} + A_{\Gamma_2,\Gamma_2} & A_{\Gamma_2,2} \\ 0 & A_{2,\Gamma_2} & A_{2,2} \end{bmatrix} \begin{bmatrix} \mathbf{u}_1 \\ \mathbf{u}_{\Gamma_1} \\ \mathbf{u}_2 \end{bmatrix} = \begin{bmatrix} \mathbf{f}_1 - A_{1,D_1}\mathbf{g}_{D_1} \\ \sum_{k=1,2}(\mathbf{f}_{\Gamma_k} - A_{\Gamma_k,D_k}\mathbf{g}_{D_k}) \\ \mathbf{f}_2 - A_{2,D_2}\mathbf{g}_{D_2} \end{bmatrix}. \quad (48)$$

Notice that we have eliminated the trace $\mathbf{u}_{\Gamma_2}$, since it coincides with $\mathbf{u}_{\Gamma_1}$.

Thanks to definition (40), the residual vectors $\mathbf{r}_{\Gamma_k}$ satisfy

$$\mathbf{r}_{\Gamma_k} = A_{\Gamma_k,k}\mathbf{u}_k + A_{\Gamma_k,\Gamma_k}\mathbf{u}_{\Gamma_k} + A_{\Gamma_k,D_k}\mathbf{g}_{D_k} - \mathbf{f}_{\Gamma_k}, \quad k = 1, 2; \quad (49)$$

hence the second row of (48) can be equivalently written as

$$\mathbf{r}_{\Gamma_1} + \mathbf{r}_{\Gamma_2} = \mathbf{0},$$

and it is the algebraic realization of (25).

We write now the algebraic form of the non-conforming problem (43).

To begin with, we analyze how to take into account the corrected definition (46) of the residuals, when $\partial\Gamma \cap \partial\Omega_D \neq \emptyset$.

Remark 9. *When $\partial\Gamma \cap \partial\Omega_D \neq \emptyset$, we define a new (very sparse) matrix $C^{(k)}$ whose non-null entries are*

$$C^{(k)}_{ij} = -\int_{\partial\Omega_{D,k}} \partial_{L_k}\varphi^{(k)}_j \varphi^{(k)}_i, \quad i \in \mathcal{I}_{\Gamma^D_k},\ j \in \mathcal{I}_{\overline{\Omega}_k} \quad (50)$$

and we adopt the same notations used above to indicate its submatrices.

Then, in order to implement (46), precisely to take into account the last integral of (46), we update the submatrices $A_{\overline{\Gamma}_k,X} = A^{(k)}(\mathcal{I}_{\overline{\Gamma}_k}, \mathcal{I}_X)$ (with $X \in \{D_k,\ \Gamma_k,\ \overline{\Gamma}_k,\ k\}$) by adding the contributions of $C^{(k)}$, i.e.

$$A_{\overline{\Gamma}_k,X} = A_{\overline{\Gamma}_k,X} + C_{\overline{\Gamma}_k,X}. \quad (51)$$

From now on, when $\partial\Gamma \cap \partial\Omega_D \neq \emptyset$, $A_{\overline{\Gamma}_k,X}$ will stand for (51).

We define two *intergrid matrices*

$$Q_{21} = R_{21}, \qquad Q_{12} = M_{\Gamma_1} R_{12} M^{-1}_{\Gamma_2}. \quad (52)$$

The algebraic counterpart of $(43)_2$ reads

$$\mathbf{u}_{\overline{\Gamma}_2} = Q_{21}\mathbf{u}_{\overline{\Gamma}_1}. \quad (53)$$

The intergrid interpolation operator Π_{12} in $(43)_3$ applies on the Lagrange expansion (42) of $(r_u)_{2,h_2}$, i.e.,

$$\sum_{i=1}^{\overline{n}_1} z^{(1)}_i \mu^{(1)}_i(\mathbf{x}) + \Pi_{12}\left(\sum_{j=1}^{\overline{n}_2} z^{(2)}_j \mu^{(2)}_j(\mathbf{x})\right) = 0, \qquad \forall \mathbf{x} \in \Gamma_1 \quad (54)$$

and, thanks to (32) and (35), the algebraic form of $(43)_3$ reads

$$\mathbf{z}_{\overline{\Gamma}_1} + R_{12}\mathbf{z}_{\overline{\Gamma}_2} = \mathbf{0} \quad \text{or, equivalently,} \quad \mathbf{r}_{\overline{\Gamma}_1} + Q_{12}\mathbf{r}_{\overline{\Gamma}_2} = \mathbf{0}, \tag{55}$$

that can be interpreted as follows:

$$\underbrace{\mathbf{r}_{\overline{\Gamma}_1}}_{dual\ d.o.f.} + M_{\Gamma_1} R_{12} M_{\Gamma_2}^{-1} \underbrace{\mathbf{r}_{\overline{\Gamma}_2}}_{dual\ d.o.f.} = \mathbf{0}.$$

$$\underbrace{\underbrace{\underbrace{\mathbf{r}_{\overline{\Gamma}_2}}_{dual\ d.o.f.}}_{Lagrange\ d.o.f}}_{interpolation}}_{dual\ d.o.f.}$$

By introducing the following submatrices: $Q_{21}^0 = Q_{21}(\mathcal{I}_{\overline{\Gamma}_2}, \mathcal{I}_{\Gamma_1})$, $Q_{21}^D = Q_{21}(\mathcal{I}_{\Gamma_2}, \mathcal{I}_{\Gamma_1^D})$, $Q_{12}^0 = Q_{12}(\mathcal{I}_{\Gamma_1}, \mathcal{I}_{\overline{\Gamma}_2})$, and by using (53), the algebraic form of (43) reads

$$\underbrace{\begin{bmatrix} A_{1,1} & A_{1,\Gamma_1} & 0 \\ A_{\Gamma_1,1} & A_{\Gamma_1,\Gamma_1} + Q_{12}^0 A_{\overline{\Gamma}_2,\overline{\Gamma}_2} Q_{21}^0 & Q_{12}^0 A_{\overline{\Gamma}_2,2} \\ 0 & A_{2,\overline{\Gamma}_2} Q_{21}^0 & A_{2,2} \end{bmatrix}}_{\mathbb{A}} \begin{bmatrix} \mathbf{u}_1 \\ \mathbf{u}_{\Gamma_1} \\ \mathbf{u}_2 \end{bmatrix} = \begin{bmatrix} \mathbf{f}_1 \\ \mathbf{f}_{\Gamma_1} + Q_{12}^0 \mathbf{f}_{\overline{\Gamma}_2} \\ \mathbf{f}_2 \end{bmatrix} - \mathbf{G}, \tag{56}$$

where the array

$$\mathbf{G} = \begin{bmatrix} \mathbf{G}_1 \\ \mathbf{G}_{\Gamma_1} \\ \mathbf{G}_2 \end{bmatrix} = \begin{bmatrix} A_{1,D_1}\mathbf{g}_{D_1} \\ A_{\Gamma_1,D_1}\mathbf{g}_{D_1} + Q_{12}^0(A_{\overline{\Gamma}_2,D_2}\mathbf{g}_{D_2} + A_{\overline{\Gamma}_2,\Gamma_2} Q_{21}^D \mathbf{g}_{\Gamma_1^D}) \\ A_{2,D_2}\mathbf{g}_{D_2} + A_{2,\Gamma_2} Q_{21}^D \mathbf{g}_{\Gamma_1^D} \end{bmatrix} \tag{57}$$

is non null only when non-homogeneous Dirichlet conditions are given on $\partial\Omega_D$ and implements the lifting of the Dirichlet datum.

The term $A_{\overline{\Gamma}_2,\Gamma_2} Q_{21}^D \mathbf{g}_{\Gamma_1^D}$ in the last two rows of (57) is justified by the fact that the trace of u_{2,h_2} on the interface Γ_2 is the interpolation through Π_{21} of the trace u_{1,h_1} on Γ_1.

System (56) represents the algebraic form of INTERNODES implemented in practice. By taking $Q_{12} = Q_{21} = I$ we recover the algebraic system (48) of the conforming case.

Notice that, even though the residuals are defined up to the boundary of Γ_k, the algebraic counterpart of condition $(43)_3$ is imposed only on the internal nodes of Γ_1. In this way the number of equations and the number of unknowns in (56) do coincide.

In the case of homogeneous Dirichlet conditions, a compact algebraic form of INTERNODES for problem (12) reads:

$$\begin{cases} A_{11}\mathbf{u}_1 = \mathbf{f}_1 - A_{1,\Gamma_1}\mathbf{u}_{\Gamma_1} \\ A_{22}\mathbf{u}_2 = \mathbf{f}_2 - A_{2,\Gamma_2}\mathbf{u}_{\Gamma_2} \\ \mathbf{u}_{\overline{\Gamma}_2} = Q_{21}\mathbf{u}_{\overline{\Gamma}_1} \\ \mathbf{r}_{\Gamma_1} + Q_{12}^0 \mathbf{r}_{\overline{\Gamma}_2} = \mathbf{0}, \end{cases}$$

with $\mathbf{r}_{\Gamma_1} = A_{\Gamma_1,1}\mathbf{u}_1 + A_{\Gamma_1,\Gamma_1}\mathbf{u}_{\Gamma_1} - \mathbf{f}_{\Gamma_1}$ and $\mathbf{r}_{\overline{\Gamma}_2} = A_{\overline{\Gamma}_2,2}\mathbf{u}_2 + A_{\overline{\Gamma}_2,\overline{\Gamma}_2}\mathbf{u}_{\overline{\Gamma}_2} - \mathbf{f}_{\overline{\Gamma}_1}$.

The instructions to build the stiffness, mass and interpolation matrices are collected in Algorithm 1, while those to assemble the matrix and the r.h.s. of system (56) and to solve it are in Algorithm 2.

Algorithm 1 Initialization of the INTERNODES matrices for 2 subdomains

for all $k = 1, 2$ **do**
  build the local stiffness matrices $A^{(k)}$;
  if $\partial\Gamma \cap \partial\Omega_D \neq \emptyset$ **then**
    build the matrices $C^{(k)}$ and update $A_{\overline{\Gamma}_k,X}$ with $X \in \{D_k,\ \Gamma_k,\ \overline{\Gamma}_k,\ k\}$ as in (51);
  end if
  build the arrays $\mathbf{f}^{(k)}$, $\mathbf{g}_{D_k}$, $\mathbf{g}_{\Gamma_k^D}$;
  build the local interface mass matrices M_{Γ_k} (formula (28));
end for
build the interpolation matrices R_{21} and R_{12} (formulas (35));
build Q_{21} and Q_{12} (formula (52));

Algorithm 2 INTERNODES for 2 subdomains: direct solver

build the matrix $\mathbb{A}$ and the r.h.s of (56);
solve the system (56) by a direct method;

2.4.1 An efficient iterative algorithm for system (56)

An alternative way to solve system (56) consists in eliminating the variables $\mathbf{u}_1$ and $\mathbf{u}_2$ from it and in solving the Schur complement system

$$S\mathbf{u}_{\Gamma_1} = \mathbf{b}, \tag{58}$$

where

$$S = S_{\Gamma_1} + Q_{12}^0 S_{\overline{\Gamma}_2} Q_{21}^0, \qquad \mathbf{b} = \mathbf{b}_{\Gamma_1} + Q_{12}^0 \mathbf{b}_{\overline{\Gamma}_2} - \mathbf{G}_{\Gamma_1}, \tag{59}$$

$$S_{\Gamma_1} = A_{\Gamma_1,\Gamma_1} - A_{\Gamma_1,1}A_{1,1}^{-1}A_{1,\Gamma_1}, \qquad S_{\overline{\Gamma}_2} = A_{\overline{\Gamma}_2,\overline{\Gamma}_2} - A_{\overline{\Gamma}_2,2}A_{2,2}^{-1}A_{2,\overline{\Gamma}_2} \tag{60}$$

$$\mathbf{b}_{\Gamma_1} = \mathbf{f}_{\Gamma_1} - A_{\Gamma_1,1}A_{1,1}^{-1}(\mathbf{f}_1 - \mathbf{G}_1), \qquad \mathbf{b}_{\overline{\Gamma}_2} = \mathbf{f}_{\overline{\Gamma}_2} - A_{\overline{\Gamma}_2,2}A_{2,2}^{-1}(\mathbf{f}_2 - \mathbf{G}_2). \tag{61}$$

S_{Γ_1} and $S_{\overline{\Gamma}_2}$ are the local Schur complement matrices, while $\mathbf{b}_{\Gamma_1}$ and $\mathbf{b}_{\overline{\Gamma}_2}$ are the local right hand sides.

System (58) can be solved, e.g., by a preconditioned Krylov method, with S_1 as preconditioner. (Notice that matrix $Q_{12}^0 S_{\overline{\Gamma}_2} Q_{21}^0$ is not a good candidate to play the role of preconditioner since it may be singular.)

Once $\mathbf{u}_{\Gamma_1}$ is known, the variables $\mathbf{u}_1$ and $\mathbf{u}_2$ are recovered by solving the local subsystems

$$\begin{aligned} A_{11}\mathbf{u}_1 &= \mathbf{f}_1 - \mathbf{G}_1 - A_{1,\Gamma_1}\mathbf{u}_{\Gamma_1}, \\ A_{22}\mathbf{u}_2 &= \mathbf{f}_2 - \mathbf{G}_2 - A_{2,\overline{\Gamma}_2}Q_{21}^0\mathbf{u}_{\Gamma_1}. \end{aligned}$$

Finally, $\mathbf{u}_{\overline{\Gamma}_1}$ is recovered by assembling $\mathbf{u}_{\Gamma_1}$ and $\mathbf{g}_{\Gamma_1^D}$ and then the numerical solution on $\overline{\Gamma}_2$ is reconstructed by the interpolation formula $\mathbf{u}_{\overline{\Gamma}_2} = Q_{21}\mathbf{u}_{\overline{\Gamma}_1}$.

The solution of system (58) can be accomplished in different ways, either by assembling explicitely the matrix S (in this case the system (58) can be solved either by direct or iterative methods), or, as usual, without assembling the Schur complement matrices S_{Γ_1}, $S_{\overline{\Gamma}_2}$ and S. In the latter case, it is sufficient to compute and store a suitable factorization of the matrices $A_{k,k}$ and dispose of a function that implements the action of S on a given array $\boldsymbol{\lambda}$.

The sketch of the algorithm to solve the Schur complement (58) by an iterative method without assembling S is reported in Algorithm 3 and Algorithm 4.

Algorithm 3 INTERNODES algorithm for 2 subdomains, iterative solution of the Schur complement $S\mathbf{u}_{\Gamma_1} = \mathbf{b}$

Build stiffness, matrix and interpolation matrices as in Algorithm 1
% *Solution step*
build the lifting $\lambda_{1,h_1} \in Y_{1,h_1}$ of $g_D|_{\Gamma_1 \cap \partial\Omega_{D,1}}$ and define the array $\boldsymbol{\lambda}_{\overline{\Gamma}_1}$ of the degrees of fredom of λ_{1,h_1} on Γ_1 (up to its boundary), as well as the subarray $\boldsymbol{\lambda}_{\Gamma_1}$ of $\boldsymbol{\lambda}_{\overline{\Gamma}_1}$ restrictred to the nodes internal to Γ_1;
compute $\boldsymbol{\lambda}_{\overline{\Gamma}_2} = Q_{21}\boldsymbol{\lambda}_{\overline{\Gamma}_1}$ and set $\boldsymbol{\lambda}_{\Gamma_2}$ the restriction of $\boldsymbol{\lambda}_{\overline{\Gamma}_2}$ to the nodes internal to Γ_2;
for all $k = 1, 2$ **do**
  solve $A_{kk}\mathbf{u}_k = \mathbf{f}_k - A_{k,D_k}\mathbf{g}_{D_k} - A_{k,\Gamma_k}\boldsymbol{\lambda}_{\Gamma_k}$;
  compute the residuals $\mathbf{r}_{\overline{\Gamma}_k} = A_{\overline{\Gamma}_k,k}\mathbf{u}_k + A_{\overline{\Gamma}_k,D_k}\mathbf{g}_{D_k} + A_{\overline{\Gamma}_k,\Gamma_k}\boldsymbol{\lambda}_{\Gamma_k} - \mathbf{f}_{\overline{\Gamma}_k}$;
end for
compute $\mathbf{b} = -(\mathbf{r}_{\Gamma_1} + Q_{12}^0\mathbf{r}_{\overline{\Gamma}_2})$;
solve $S\mathbf{u}_{\Gamma_1} = \mathbf{b}$ by an iterative matrix-free method, (see Algorithm 4 for the computation of $\mathbf{v} = S\mathbf{p}_{\Gamma_1}$, for a given $\mathbf{p}_{\Gamma_1}$);
recover $\mathbf{u}_{\overline{\Gamma}_1}$ by assembling $\mathbf{u}_{\Gamma_1}$ and $\mathbf{g}_{\Gamma_1^D}$;
compute $\mathbf{u}_{\overline{\Gamma}_2} = Q_{21}\mathbf{u}_{\overline{\Gamma}_1}$;
for all $k = 1, 2$ **do**
  solve $A_{kk}\mathbf{u}_k = \mathbf{f}_k - A_{k,D_k}\mathbf{g}_{D_k} - A_{k,\Gamma_k}\mathbf{u}_{\Gamma_k}$;
end for

Algorithm 4 Evaluation of $\mathbf{v} = S\mathbf{p}_{\Gamma_1}$, where $\mathbf{p}_{\Gamma_1}$ is the array of the dof of a discrete function that is null on $\partial\Gamma_1$

compute $\mathbf{p}_{\overline{\Gamma}_2} = Q_{21}^0\mathbf{p}_{\Gamma_1}$;
for all $k = 1, 2$ **do**
  solve $A_{kk}\mathbf{u}_k = -A_{k,\Gamma_k}\mathbf{p}_{\Gamma_k}$;
  compute the residuals $\mathbf{r}_{\overline{\Gamma}_k} = A_{\overline{\Gamma}_k,k}\mathbf{u}_k + A_{\overline{\Gamma}_k,\Gamma_k}\mathbf{p}_{\Gamma_k}$;
end for
compute $\mathbf{v} = \mathbf{r}_{\Gamma_1} + Q_{12}^0\mathbf{r}_{\overline{\Gamma}_2}$;

2.5 Accuracy of INTERNODES

Under the assumptions that problem (5) is well posed (see, e.g., [22, 11]) the following convergence theorem, establishing the optimal error bound for the INTERNODES method with respect to the mesh sizes h_1 and h_2, is proved in [11], in the case of homogeneous boundary data, straight interfaces, when the intergrid operators Π_{12} and Π_{21} are the classical Lagrange interpolation operators and when $\partial\Gamma \cap \partial\Omega_D = \emptyset$.

Theorem 1. *Assume that the solution u of problem (7) belongs to $H^s(\Omega)$, for some $s > 3/2$, that $\lambda = u_{|\Gamma} \in H^\sigma(\Gamma)$ for some $\sigma > 1$ and that $r_2 = \partial_{L_2} u_2 \in H^\nu(\Gamma)$ for some $\nu > 0$. Then there exist $q \in [1/2, 1[$, $z \in [3/2, 2[$, and a constant $c > 0$ independent of both h_1 and h_2 s.t.*

$$\begin{aligned} \|u - u_h\|_* \leq \; & c \left\{ \left(h_1^{\varrho_1 - 1/2} \left(1 + (h_2/h_1)^q\right) + h_2^{\varrho_2 - 1/2} \right) \|\lambda\|_{H^\sigma(\Gamma)} \right. \\ & + \sum_{k=1,2} h_k^{\ell_k - 1} (\|u_k\|_{H^s(\Omega_k)} + \|\lambda\|_{H^{s-1/2}(\Gamma)} + \|f\|_{H^{s-2}(\Omega_k)}) \\ & \left. + \left[\alpha h_1^{\zeta_1 + 1/2} + \left(1 + (h_1/h_2)^z\right) h_2^{\zeta_2 + 1/2} \right] \|\partial_{L_2} u_2\|_{H^\nu(\Gamma)} \right\}, \end{aligned} \tag{62}$$

where $\ell_k = \min(s, p_k + 1)$ for $k = 1, 2$, $\varrho_k = \min(\sigma, p_k + 1)$, $\zeta_k = \min(\nu, p_k + 1)$, $\alpha = 1$ if $\nu > 1$ and $\alpha = 0$ otherwise.

We notice that, when $h_1, h_2 \to 0$, if the ratio h_2/h_1 is uniformly bounded from above and below, then INTERNODES exhibits optimal accuracy, i.e. the accuracy of the primal finite element spaces X_{k,h_k} used to discretize the local subproblems.

The convergence analysis w.r.t. the local polynomial degrees p_1 and p_2 is an open problem, nevertheless numerical results (see the next sections) show that INTERNODES exhibits optimal accuracy also w.r.t. to p_1 and p_2.

Remark 10. *Numerical results (see the next Section) show that the error bound (62) is respected also when $\partial\Gamma \cap \partial\Omega_D \neq \emptyset$.*

Even if the Lagrange interpolation is employed heavily to prove Theorem 1, INTERNOES can achieve the optimal order of convergence also when supported by other types of interpolation, provided that they are accurate enough w.r.t. the discretization subspaces V_{k,h_k}. The numerical results of Sect. 2.6.2 show the effectiveness of RL-RBF interpolation in the case of a curved interface and polynomial degrees $p \leq 5$.

2.6 Numerical results for 2 subdomains

We provide numerical evidence to the error estimate reported above in (62). We consider two test cases, one in 2D and one in 3D. In each case we consider the case of a fully Finite Element discretization (FEM/FEM) and that of a fully Spectral Element discretization (SEM/SEM). In the 2D case we consider also an hybrid case FEM/SEM showing the robustness of INTERNODES.

2.6.1 Test case #1

Let us consider the differential problem (5) in $\Omega = (0,2) \times (0,1)$ with $Lu = -\Delta u + u$ and f, g_D and g_N such that the exact solution is

$$u(x,y) = \arctan(4(x-3/2))\cos((y-x/2)\pi) + 1,$$

then we impose Neumann boundary condition on $\partial\Omega_N = (0,2) \times \{1\}$ and Dirichlet conditions on $\partial\Omega_D = \partial\Omega \setminus \partial\Omega_N$.

The computational domain Ω is split in $\Omega_1 = (0,1)^2$ and $\Omega_2 = (0,1) \times (1,2)$ and

$$u_h = \begin{cases} u_{1,h_1} & \text{in } \Omega_1 \\ u_{2,h_2} & \text{in } \Omega_2 \end{cases} \tag{63}$$

denotes the numerical solution computed with INTERNODES.

In Fig. 8 we show the numerical solutions obtained in the case of FEM-FEM (left) and SEM-SEM (right) coupling. The solution drawn in the left picture is obtained with FEM$-\mathbb{P}_1$ discretization in each subdomain with mesh sizes $h_1 = 1/10$ and $h_2 = 1/19$, while that drawn in the right picture has been computed with SEM of degree $p_1 = 4$ and mesh-size $h_1 = 1/3$ in Ω_1 and SEM with degree $p_2 = 6$ and mesh-size $h_2 = 1/5$ in Ω_2.

In Fig. 9 we show the broken-norm errors between the INTERNODES solution u_h and the exact one u:

$$\|u_h - u\|_* = \left(\sum_{k=1,2} \|u_h - u\|^2_{H^1(\Omega_k)} \right)^{1/2}. \tag{64}$$

The INTERNODES solutions producing the errors plotted in the left picture of Fig. 9 are computed with $h_2 \sim h_1/2$ and the same polynomial degree $p = p_1 = p_2$. FEM$-\mathbb{P}_1$ are considered when $p = 1$ and SEM$-\mathbb{Q}_p$ otherwise.

The INTERNODES solutions providing the errors plotted in Fig. 9 are computed with three different configurations that are described in the caption of the figure itself.

When the mesh sizes h_1 and h_2 tend to zero, the errors plotted in the left picture of Fig. 9 dacay obeying to the convergence estimate (62). In such a case the ratio h_1/h_2 is uniformly bounded and the errors are governed by the term $(h_1^{p_1} + h_2^{p_2})$ (notice that the solution is infinitely differentiable).

In the right picture of Fig. 9 we show the errors w.r.t. the local polynomial degrees. In this case, the convergence rate w.r.t. the polynomial degree is more than algebraic, as a matter of fact it is of exponential type, as typical in SEM. The proof of this result is an open problem.

2.6.2 Test case #2

With this example we aim at showing the robustness of INTERNODES when the discretization from one side of the interface is very coarse with respect to the discretization on the other side, as well as the effectiveness of RL-RBF interpolation.

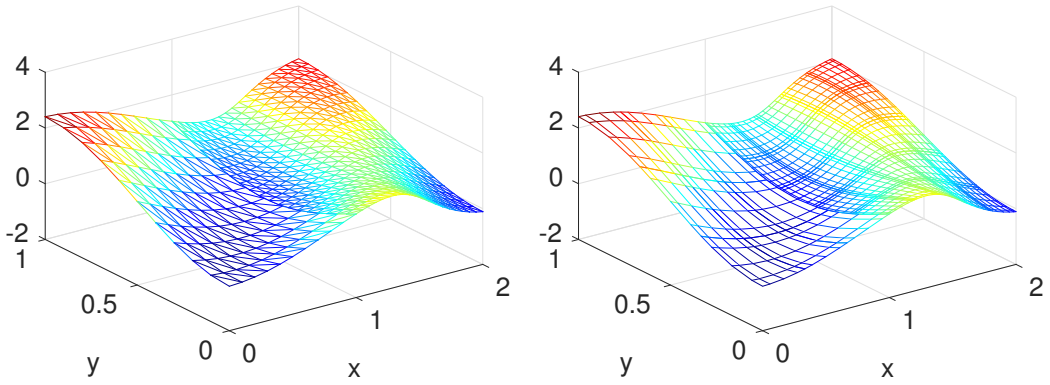

Figure 8: *Test case #1.* At left, the INTERNODES solution obtained with FEM-FEM discretization, $p_1 = p_2 = 1$ and $h_1 = 1/10$, $h_2 = 1/19$. At right, the INTERNODES solution obtained with SEM-SEM discretization, polynomial degrees $p_1 = 4$, $p_2 = 6$ and mesh sizes $h_1 = 1/3$, $h_2 = 1/5$

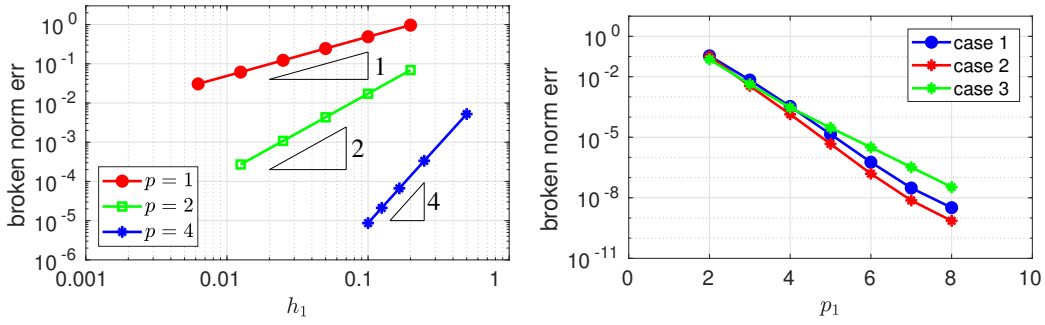

Figure 9: *Test case #1.* At left, the broken-norm errors (64) versus h_1, with $h_2 \sim h_1/2$ and $p_1 = p_2 = p$. When $p = 1$, FEM-$\mathbb{P}_1$ are used inside each subdomain, while when $p > 1$ SEM are used inside each subdomain. At right, the broken-norm errors (64) versus the polynomial degree p_1 in Ω_1 for SEM-SEM discretization with: $p_2 = p_1 + 2$, $h_1 = 1/4$, $h_2 = 1/7$ (case 1), $p_2 = p_1 - 1$, $h_1 = 1/5$, $h_2 = 1/8$ (case 2), and $p_2 = p_1$, $h_1 = 1/5$, $h_2 = 1/3$ (case 3)

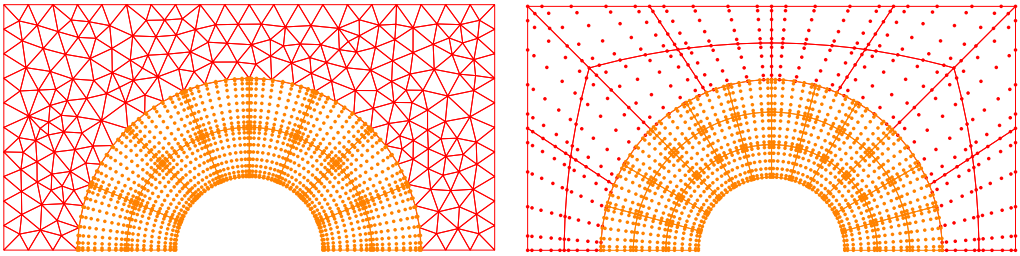

Figure 10: The hybrid FEM-SEM (at left) and SEM-SEM (at right) meshes used in the *Test case #2*

We approximate the solution of problem (5) with $Lu = -\Delta u$ in the domain Ω drawn in Fig. 1, right. More precisely, denoting by C_0 the circle centered in (0,0) and with radius $r_0 = 0.3$, we set $\Omega = ((-1,1) \times (0,1)) \setminus C_0$. The functions f, g_D and g_N are defined so that the exact solution is

$$u(x,y) = \sin(1.5/\sqrt{x^2+y^2})(x-y),$$

then Neumann conditions are imposed on the horizontal sides of Ω and Dirichlet conditions on $\partial\Omega \setminus \partial\Omega_N$.

We define the circle C_1 centered in (0,0) with radius $r_1 = 0.7$, then we split Ω into two subdomains $\Omega_1 = \Omega \setminus C_1$ and $\Omega_2 = \Omega \cap C_1$.

Since the interface Γ is curved, the RL-RBF interpolation matrices (38) are employed.

First, we consider a hybrid coupling with FEM-$\mathbb{P}_1$ (with $h_1 = 1/10$) in Ω_1 and SEM-$\mathbb{Q}_{10}$ in Ω_2 (with 16 elements) as shown in Fig. 10, left.

The INTERNODES solution computed with $h_1 = 1/10$ in Ω_1 and local polynomial degree equal to $p_2 = 10$ in Ω_2 is shown in Fig. 11, left. The corresponding broken-error norm is about $8.55 \cdot 10^{-2}$.

In the right picture of Fig. 11 we show the broken-norm error as well as the H^1-norm errors inside each subdomains versus the $\mathbb{P}_1$ mesh size h_1 in Ω_1. It is evident that the error is larger inside the FEM domain Ω_1 where the discretization is coarser. By refining the FEM mesh the broken-norm errors decay linearly w.r.t. h_1 (as a matter of fact they coincide with the H^1-norm errors in Ω_1), while the H^1-norm errors in Ω_2 decay slightly faster, thanks to the higher accuracy of SEM. We warn the reader that the numerical solution u_{2,h_2} in Ω_2 does not exploits the optimal exponential accuracy typical of SEM since u_{2,h_2} depends on the less accurate solution u_{1,h_1} computed in Ω_1.

We consider now the SEM-SEM coupling in order to test the influence (if any) of RL-RBF on the accuracy of INTERNODES. We decompose both Ω_1 and Ω_2 in four quads with curved edges, corresponding to $h_1 = h_2 = 1$ and local polynomial degree p_k, then we refine each of them by dividing it in $ne_k \times ne_k$ quads, with $ne_1 \neq ne_2$. The meshes $\mathcal{T}_{1,h_1}$ (red) and $\mathcal{T}_{2,h_2}$ (orange), corresponding to $ne_1 = 2$, $ne_2 = 3$, $p_1 = 5$ and $p_2 = 6$ are shown in Fig. 10, right.

To begin, we fix $p_1 = p_2$ and we compute the INTERNODES solution with $ne_1 =$

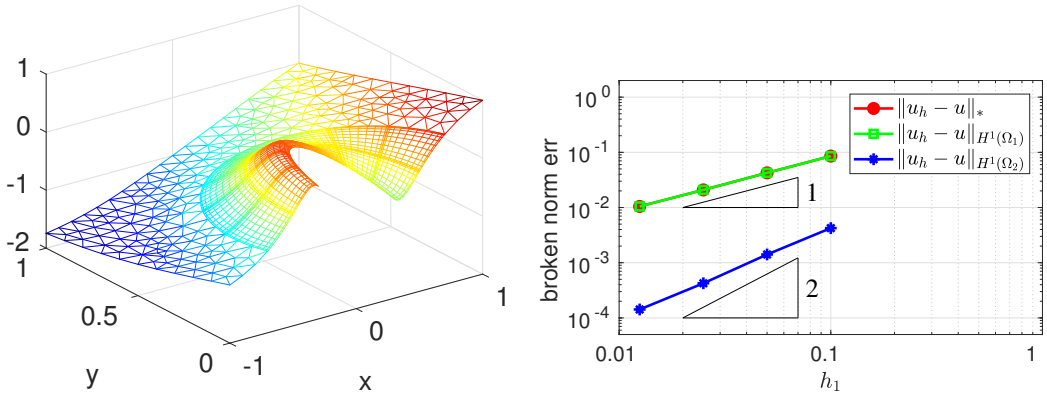

Figure 11: *Test case #2.* At left, the INTERNODES solution obtained with FEM-SEM discretization, $p_1 = 1$ and $h_1 = 1/10$ in Ω_1, $p_2 = 10$ and 16 spectral elements in Ω_2. At right, the errors versus the mesh size h_1 of the triangulation in Ω_1. The broken-norm error and the H^1-norm error in Ω_1 coincide

$1, \ldots, 10$, $ne_2 = ne_1 + 1$. The broken-norm errors versus $h_1 = 1/ne_1$ are shown in Fig. 12, left, for $p = 2, 3, 5$, they behave almost as h_1^p.

Then, we fix $ne_1 = 2$ and $ne_2 = 3$ and we compute the INTERNODES solution with $p_1 = 2, \ldots, 8$ and $p_2 = p_1 + 1$. The corresponding broken-norm errors are shown in Fig. 12, right; they decay more than algebraically, but the convergence rate depends on the radius r used to set-up the RL-RBF interpolation. The larger r the smaller the error, but the error curves show a plateau for increasing p. (Notice that, when both p and r are large, the condition number of the matrices Φ_{kk} that are involved in the computation of R_{12} and R_{21} (38) can be very large.)

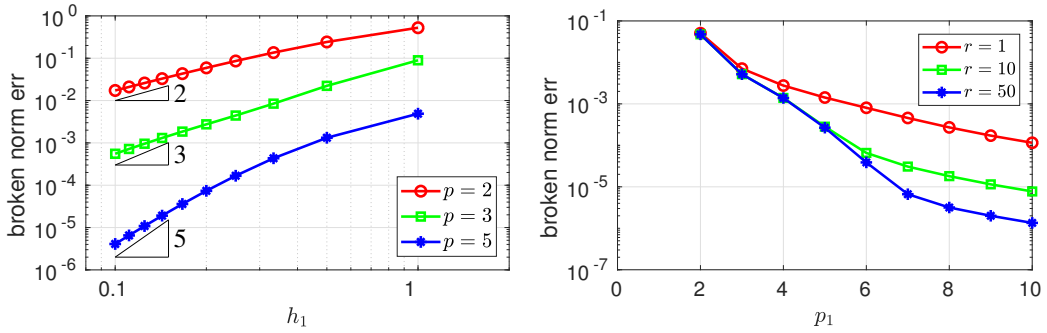

Figure 12: *Test case #2.* At left, the broken-norm errors for SEM-SEM discretization versus the mesh size h_1 of the mesh in Ω_1. At right, the broken-norm errors for SEM-SEM discretization versus the polynomial degree p_1 in Ω_1. r is the radius of RL-RBF used to set-up the iterpolation matrices of INTERNODES

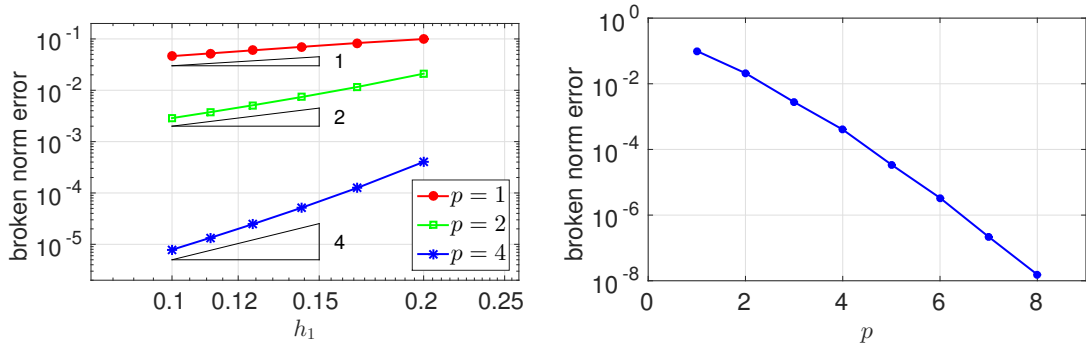

Figure 13: *Test case #3.* The broken-norm error w.r.t. the mesh-size h_1 with $p = p_1 = p_2$ fixed (left) and w.r.t. the local polynomial degree $p = p_1 = p_2$, with fixed mesh size (right) $h_1 = 1/5$ and $h_2 = 1/3$.

2.6.3 Test case #3

We approximate the solution of problem (5) with $\alpha = 1$ and $\gamma = 0$ in the 3D domain $\Omega = (0, 2) \times (0, 1) \times (0, 1)$. Dirichlet boundary conditions are imposed on the whole boundary $\partial\Omega$ and the data f and g_D are set in such a way that the exact solution is $u(x, y, z) = (y^2 - y)(z^2 - z)\sin(xyz\pi)$.

Ω is decomposed into two subdomains $\Omega_1 = (0, 1)^3$ and $\Omega_2 = (1, 2) \times (0, 1) \times (0, 1)$ and in each subdomain we consider either FEM$-\mathbb{P}_1$ (tetrahedral elements) or SEM-$\mathbb{Q}_p$ (hexahedral elements).

In each Ω_k (for $k = 1, 2$) we consider a partition in $6(ne_k \times ne_k \times ne_k)$ tetrahedra when $p = 1$, and in $(ne_k \times ne_k \times ne_k)$ hexahedra when $p > 1$. Then the non-conformity is established by setting $ne_2 = ne_1 - 2$ (with $ne_1 > 2$). We define $h_k = 1/ne_k$, for $k = 1, 2$, thus $h_2 = h_1/(1 - 2h_1)$.

In Fig. 13, the errors in broken-norm are shown, w.r.t. both the mesh size h_1 of Ω_1 and the local polynomial degree $p = p_1 = p_2$. We observe that they behave as in the Test case #1, obeying to the convergence estimate (62) when $h_1,\ h_2 \to 0$. Moreover, the errors decay spectrally when p increases, as for 2D problems.

2.7 INTERNODES for decomposition with $M > 2$ subdomains

Let Ω_k, $k = 1, \ldots, M$, denote a family of disjoint subdomains s.t. $\cup_k \overline{\Omega}_k = \overline{\Omega}$. Let us suppose that each Ω_k is convex with Lipschitz boundary $\partial\Omega_k$ (for $k = 1, \ldots, M$), and that any angle between two consecutive edges is less than π. Let $\Gamma_k = \partial\Omega_k \setminus \partial\Omega$ be the part of the boundary of Ω_k internal to Ω, and $\Gamma_{k\ell} = \Gamma_{\ell k} = \partial\Omega_k \cap \partial\Omega_\ell$ be the interface between the two subdomains Ω_k and Ω_ℓ. Finally, let $\Gamma = \cup_{k,\ell}\Gamma_{k\ell}$ be the skeleton of the decomposition. Intersections reduced to a single point are considered empty. (Two simple decompositions are shown in Fig. 14, while an example of a more general decomposition is shown in Fig. 15, left.)

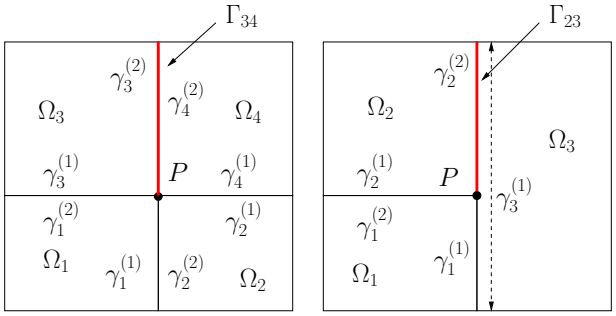

Figure 14: Two simple decompositions

The multidomain formulation of problem (5) reads:

$$\begin{cases} Lu_k = f & \text{in } \Omega_k, \quad k = 1, \ldots, M \\ u_k = u_\ell, & \text{on } \Gamma_{k\ell}, \\ \partial_{L_k} u_k + \partial_{L_\ell} u_\ell = 0 & \text{on } \Gamma_{k\ell}, \\ u_k = g_D & \text{on } \partial\Omega_{D,k}, \\ \partial_{L_k} u_k = g_N & \text{on } \partial\Omega_{N,k}. \end{cases} \tag{65}$$

Let $\gamma_k^{(t)} \subset \Gamma_k$ be the $t-$th edge of Γ_k (the sub-index k identifies the domain, while t is the index of the edge of $\partial\Omega_k$ among all edges of Γ_k).

We denote by $\gamma_k^{(t)}$ and $\gamma_\ell^{(q)}$ the two edges of Ω_k and Ω_ℓ whose intersection is $\Gamma_{k\ell} = \Gamma_{\ell k} \neq \emptyset$.

In the example of Fig. 14, left, we have $\Gamma_{k\ell} = \gamma_k^{(t)} = \gamma_\ell^{(q)}$ for any interface $\Gamma_{k\ell}$ of the decomposition, while in the example depicted in Fig. 14, right, we have $\Gamma_{12} = \gamma_1^{(2)} = \gamma_2^{(1)}$, $\Gamma_{23} = \gamma_2^{(2)} \subset \gamma_3^{(1)}$ and $\Gamma_{13} = \gamma_1^{(1)} \subset \gamma_3^{(1)}$.

Between $\gamma_k^{(t)}$ and $\gamma_\ell^{(q)}$, one is tagged as *master* and the other as *slave* and we define the skeleton

$$\Gamma^{(m)} = \bigcup_{\substack{k,t\,: \\ \gamma_k^{(t)} \text{ is master}}} \gamma_k^{(t)}, \tag{66}$$

that in the mortar community is named *mortar interface*.

A-priori there is no constraint in tagging an edge as either master or slave. In the example of Fig. 14 right, we could tag as master the edge $\gamma_3^{(1)}$ (in which case $\gamma_1^{(1)}$ and $\gamma_2^{(2)}$ will be slave), or other way around.

In each Ω_k we consider a suitable triangulation and the corresponding finite dimensional spaces (as introduced in Section 2.2) that are totally independent of the discretizations inside the adjacent subdomains.

In order to write the INTERNODES method, we need to generalize the definition of the residual (46) on the edge $\gamma_k^{(t)}$ (either slave or master) as follows.

First of all, for each $\gamma_k^{(t)} \subset \Gamma_k$ (either slave or master), we define the set $G_k^{(t)} = \partial\Omega_k \setminus (\mathring{\gamma}_k^{(t)} \cup \partial\Omega_{N,k})$. For any i s.t. $\mathbf{x}_i^{(\gamma_k^{(t)})} \in \partial\gamma_k^{(t)} \cap G_k^{(t)}$, we define the real numbers

$$(r_u^{(k)})_i = \quad a_k(u_{k,h_k}, \overline{\mathcal{R}}_k\mu_i^{(k)}) - \mathcal{F}_k(\overline{\mathcal{R}}_k\mu_i^{(k)}) - \int_{G_k^{(t)}} \partial_{L_k} u_{k,h_k}\ \overline{\mathcal{R}}_k\mu_i^{(k)}, \tag{67}$$

that generalize those defined in (46). Then, we define the coefficients $(z_u^{(k)})_j$ and the discrete residuals as in (41) and (42), respectively.

As for the 2-domains situation, the last term of (67) guarantees that the residual function $(r_u)_{k,h_k}$ is the discrete flux associated with the function u_{k,h_k} across the interface $\gamma_k^{(t)}$.

The weak form of INTERNODES applied to (65) reads: for $k = 1, \ldots, M$ find $u_{k,h_k} \in X_{k,h_k}$ with $u_{k,h_k} = g_{D,h_k}$ on $\partial\Omega_{D,k}$ (g_{D,h_k} is a suitable approximation of g_D) such that

$$\begin{cases} a_k(u_{k,h_k}, v_{k,h_k}) = \mathcal{F}_k(v_{k,h_k}) & \forall v_{k,h_k} \in V_{k,h_k}^0, \quad k = 1, \ldots, M, \\ u_{\ell,h_\ell} = \Pi_{\ell k} u_{k,h_k} & \text{on any } \gamma_\ell^{(q)} \text{ slave}: \ \gamma_\ell^{(q)} \cap \gamma_k^{(t)} \neq \emptyset, \\ (r_u)_{k,h_k} + \Pi_{k\ell}(r_u)_{\ell,h_\ell} = 0 & \text{on any } \gamma_k^{(t)} \text{ master}: \ \gamma_\ell^{(q)} \cap \gamma_k^{(t)} \neq \emptyset. \end{cases} \tag{68}$$

Remark 11. *Notice that each cross-point (i.e. a vertex shared by more than two subdomains) always belongs to the skeleton $\Gamma^{(m)}$ since it is the end-point of at least one master edge (see Fig. 15). Cross-points shared by two (or several) master edges (like the black circles in Figs. 15, left) hold a single degree of freedom (that is, the finite element solution is continuous therein). Moreover, since a cross-point is always an interpolation node (as it is the endpoint of almost two edges), the value of the trace there is preserved when passing from the master edge to the slave one.*

If $\gamma_k^{(t)}$ and $\gamma_\ell^{(q)}$ are the master and the slave sides, respectively, and their intersection is $\Gamma_{k\ell}$, then $R_{(\ell,q),(k,t)}$ is the interpolation matrix that maps the master side to the slave one (it plays the role of matrix R_{21} defined in (35)), while $R_{(k,t),(\ell,q)}$ is the interpolation matrix from the slave to the master side (as R_{12} in (35)).

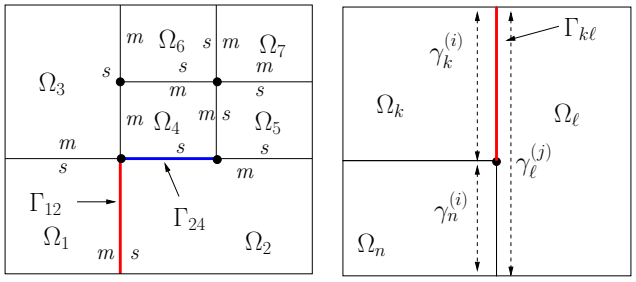

Figure 15: A partition of Ω into 7 subdomains (left figure). The letters m and s denote the choice made for the master and slave sides, the black circles denote the cross-points. Description of interfaces and edges (right)

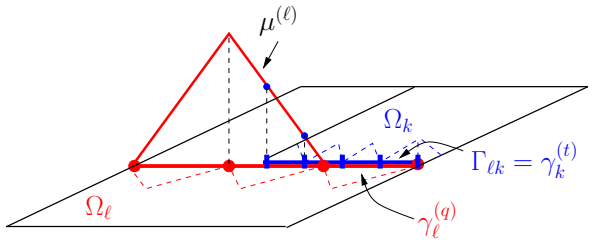

Figure 16: The basis function $\mu^{(\ell)}$ (in red) is associated with a node of $\gamma_\ell^{(q)}$ that does not belong to $\Gamma_{\ell k} = \gamma_k^{(t)} \cap \gamma_\ell^{(q)}$, nevertheless its support intersects the interface $\Gamma_{k\ell}$ and $\mu^{(\ell)}$ must be taken into account in assembling the matrix $R_{(k,t),(\ell,q)}$

When the measure of $\gamma_\ell^{(q)}$ is larger than that of $\gamma_k^{(t)}$ (as, e.g., $\gamma_3^{(1)}$ and $\gamma_2^{(2)}$ in Fig. 14, right), all the basis functions of $\gamma_\ell^{(q)}$ whose support has non-empty intersection with $\gamma_k^{(t)}$ must be taken into account when building $R_{(k,t),(\ell,q)}$, included those basis functions associated with the nodes that do not belong to $\Gamma_{k\ell}$ (i.e. Γ_{23} in the case of Fig. 14, right, see also Fig. 16). Alternatively, one can build the interface mass matrices and the interpolation matrices on the larger edge (as $\gamma_3^{(1)}$ in the case of Fig. 14, right), by assembling the contributions arising from the shorter edges of the opposite side of the interface (as $\gamma_1^{(1)}$ and $\gamma_2^{(2)}$ in the case of Fig. 14, right).

The degrees of freedom of the global multidomain problem are the values of u_h at the nodes of $\Gamma^{(m)}$ jointly with the degrees of freedom internal to each Ω_k and those on the Neumann boundary. As done in Section 2.4.1, we eliminate the degrees of freedom with index in $\mathcal{I}_k$ and solve the Schur complement system (analogous to (58))

$$S\mathbf{u}_{\Gamma^{(m)}} = \mathbf{b} \tag{69}$$

by, e.g., a Krylov method. Notice that usually the matrix S is not assembled, but it is sufficient to provide a function that computes the matrix-vector product $\mathbf{v} = S\mathbf{p}$, for a given $\mathbf{p}$ approximating $\mathbf{u}_{\Gamma^{(m)}}$ (see [11, Algorithm 2]).

2.8 Numerical results for $M > 2$ subdomains.

In this Section we apply INTERNODES to an infinitely differentiable test solution and to the Kellogg's test case with jumping coefficients, showing that also in the case of decompositions with several subdomain INTERNODES attains optimal rate of convergence (as stated by the error estimate (62)).

2.8.1 The "four and a half tatami" test case

Let us consider the differential problem (5) in $\Omega = (0,3) \times (0,3)$ with $Lu = -\Delta u + u$ and f and g_D such that the exact solution is

$$u(x,y) = \cos((x+y)\pi/2)(x-2y).$$

Then we impose Dirichlet boundary condition on $\partial\Omega_D = \partial\Omega$.

The computational domain Ω is split into 5 subdomains as in a typical disposition of "four and a half tatami" (see Fig. 17, left), and inside each subdomain we consider either FEM or SEM discretization, one independent eachother. More precisely, $\Omega_1 = (0,1)\times(0,2)$, $\Omega_2 = (1,3)\times(0,1)$, $\Omega_3 = (2,3)\times(1,3)$, $\Omega_4 = (0,2)\times(2,3)$ and $\Omega_5 = (1,2)^2$.

In Fig. 17, right, we show the numerical solution computed with a hybrid FEM-SEM discretization, precisely SEM-$\mathbb{Q}_4$ in Ω_1 and in Ω_3, FEM-$\mathbb{P}_1$ in Ω_2, in Ω_4, and in Ω_5 (in each subdomain the mesh is taken uniform and regular).

In Fig. 18 the errors (64) are drawn for both full non-conforming FEM$-\mathbb{P}_1$ and full non-conforming SEM$-\mathbb{Q}_p$ discretizations, showing that INTERNODES attains optimal order of convergence (as stated in (62)), also for decompositions with more than two subdomains and internal cross-points.

The errors drawn in the left picture of Fig. 18 refer to the INTERNODES numerical solution computed with $h_1 = 1/k$ with $k \in \{5, 10, 30, 40, 80, 100\}$ and: $h_2 = 2/(3k-1)$, $h_3 = 1/(2k)$, $h_4 = 2/(3k+1)$, and $h_5 = 1/(k+5)$, so that the meshes are non-conforming across all the interfaces. The maximum mesh-size h_{max} in the whole domain Ω coincides with h_1, while the minimum mesh-size $h_{min} = h_5$. In the case of $p = 1$ we have plot the errors versus either h_{max} (red curve) and h_{min} (green curve), as well as the error obtained by a conforming discretization with the same h in the whole domain Ω (blue curve).

These results highlight that, although INTERNODES is based on interpolation operators rather than projections (as in the mortar methods), the best approximation error of the finite element discretization is preserved and not downgraded.

The error curve drawn in the right picture of Fig. 18 refers to the INTERNODES numerical solution computed with SEM$-\mathbb{Q}_p$, with: p_1 in the range $[2, 8]$ and $p_2 = p_1+1$, $p_3 = p_1 - 1$, $p_4 = p_1 + 1$, $p_5 = p_1 + 2$; $h_1 = 1/4$, $h_2 = 1/2$, $h_3 = 1/7$, $h_4 = 2/5$ and $h_5 = 1/2$. As in the case of decomposition with only two subdomains, the error decays with spectral accuracy when all the polynomials degree increase.

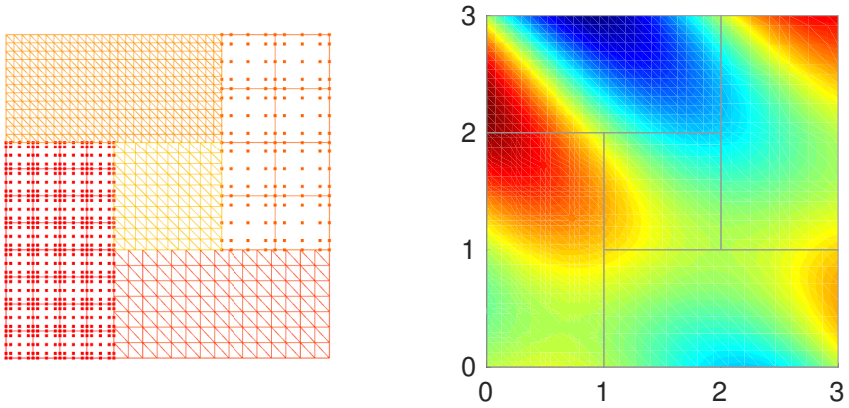

Figure 17: At left, the hybrid FEM-SEM mesh for the "four and a half tatami" test case. At right, the corresponding numerical solution

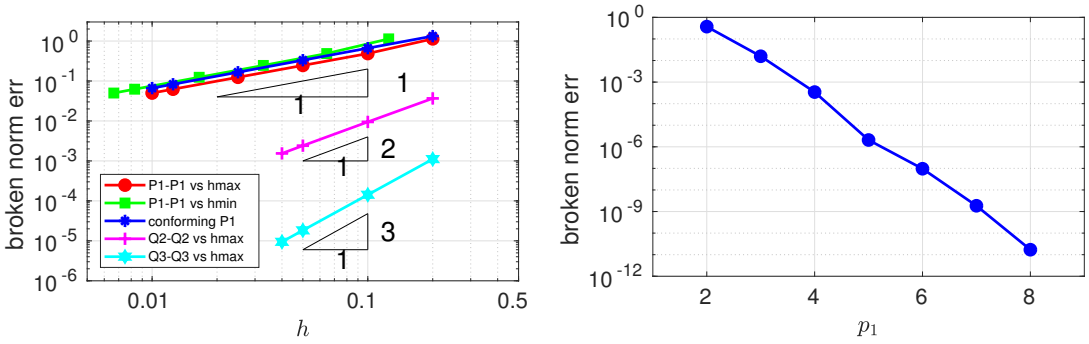

Figure 18: The errors (64) for the "four and a half tatami" test case. At left, the broken-norm errors versus the mesh size h, for both FEM-FEM (non-conforming $\mathbb{P}_1$ in both subdomains) and SEM-SEM (non-conforming $\mathbb{Q}_p$ with $p = 2, 3$ in both subdomains); the error provided by conforming $\mathbb{P}_1$ is plotted for a comparison. At right, the broken-norm errors versus the polynomial degree for SEM-SEM

2.8.2 The Kellogg's test case

This is a very challenging problem whose solution features low regularity. The so-called Kellogg's function (see, e.g., [20]) is an exact weak solution of the elliptic problem

$$\begin{cases} -\nabla \cdot (\alpha \nabla u) = 0 & \text{in } \Omega = (-1,1)^2 \\ u = g_D & \text{on } \partial\Omega, \end{cases} \tag{70}$$

with piece-wise constant coefficient α: $\alpha = R > 0$ in the first and the third quadrants, and $\alpha = 1$ in the second and in the fourth ones. The solution u can be written in terms of the polar coordinates r and θ as $u(r, \theta) = r^\gamma \mu(\theta)$, where $\gamma \in (0, 2)$ is a given parameter, while $\mu(\theta)$ is a $2\pi-$periodic continuous function (more regular only when $\gamma = 1$) defined as follows:

$$\mu(\theta) = \begin{cases} \cos((\pi/2 - \sigma)\gamma)\cos((\theta - \pi/2 + \rho)\gamma) & 0 \le \theta \le \pi/2 \\ \cos(\rho\gamma)\cos((\theta - \pi + \sigma)\gamma) & \pi/2 \le \theta \le \pi \\ \cos(\sigma\gamma)\cos((\theta - \pi - \rho)\gamma) & \pi \le \theta \le 3\pi/2 \\ \cos((\pi/2 - \rho)\gamma)\cos((\theta - 3\pi/2 - \sigma)\gamma) & 3\pi/2 \le \theta \le 2\pi. \end{cases} \tag{71}$$

The parameters σ, ρ, γ and the coefficient R (that is involved in the definition of α) must satisfy the following non-linear system:

$$\begin{cases} R = -\tan((\pi/2 - \sigma)\gamma)\cot(\rho\gamma) \\ \frac{1}{R} = -\tan(\rho\gamma)\cot(\sigma\gamma) \\ R = -\tan(\sigma\gamma)\cot((\pi/2 - \rho)\gamma) \\ 0 < \gamma < 2 \\ \max\{0, \pi\gamma - \pi\} < 2\gamma\rho < \min\{\gamma\pi, \pi\} \\ \max\{0, \pi - \gamma\pi\} < -2\gamma\sigma < \min\{\pi, 2\pi - \gamma\pi\}. \end{cases} \tag{72}$$

After choosing $\rho = \pi/4$, and $\gamma \in \{0.4, 0.6, 1.4, 1.6\}$ and by solving the non-linear system (72), we obtain the values of R and σ reported in Table 1.

Table 1: The parameters for the Kellogg's test case, when $\rho = \pi/4$

γ	R	σ
0.4	9.472135954999585	-3.141592653589793
0.6	3.851839996319182	-1.832595714594046
1.4	0.2596161836824997	-0.3365992128846207
1.6	0.1055728090000841	-0.1963495408493620

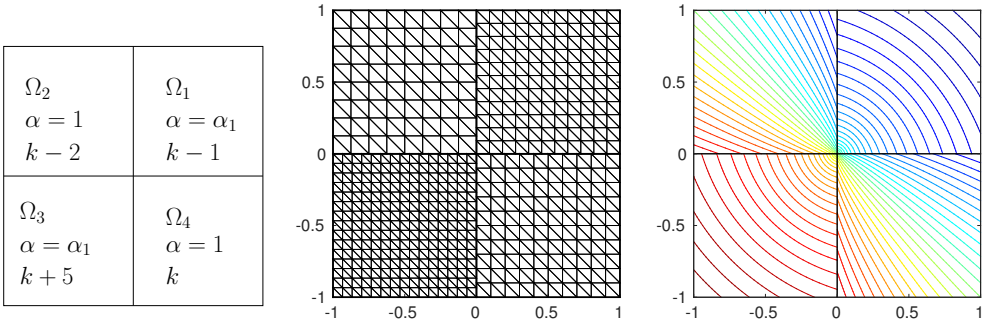

Figure 19: At left, the decomposition of Ω into four subdomains. In the middle, the nonconforming $\mathbb{P}_1$ meshes for $k = 10$. At right, the Kellogg's solution with $\gamma = 0.4$ and $R = 9.472135954999585$ computed by INTERNODES and $\mathbb{P}_1$

The case $\gamma = 1$ is trivial since the solution is a plane. When $\gamma \neq 1$, $u \in H^s(\Omega)$, with $s = 1 + \gamma - \varepsilon$ for any $\varepsilon > 0$; the solution features low regularity at the origin and its normal derivatives to the axis are discontinuous.

We solve problem (70) by applying INTERNODES to the 4-subdomains decomposition induced by the discontinuity of α and by using either $\mathbb{P}_1$ or $\mathbb{Q}_2$ finite elements in each subdomain (see the $\mathbb{P}_1$ mesh in Fig. 19). The meshes at the interfaces are non-conforming as shown in Figure 19, more precisely given $k \in \mathbb{N}$, the subdomains mesh-sizes are: $h_1 = 1/(k-1)$, $h_2 = 1/(k-2)$, $h_3 = 1/(k+5)$ and $h_4 = 1/k$.

By refining the meshes (we cycle on $k = 20,\ 40,\ 80,\ 160$), we measure the convergence order of INTERNODES on the Kellogg's solution for different values of the parameter γ. The results are shown in Table 2 and the convergence estimate provided by Theorem 1 for two subdomains is here confirmed, although this test case involves four subdomains instead of two.

3 Fluid filtration in porous media (the Stokes-Darcy coupling)

Flow processes in a free-fluid region adjacent to a porous medium occur in many relevant applications. At the microscopic scale the complete process can in principle be modelled by the Navier-Stokes equations both in the free-fluid and in the porous

Table 2: Convergence orders of INTERNODES for the Kellogg's test solution. The case $\gamma = 0.4$ is not covered by the convergence Theorem 1 since $s < 3/2$. The experimental convergence orders are shown in the last two columns

γ	$s = 1 + \gamma - \varepsilon$ s.t. $u \in H^s(\Omega)$	theoretical convergence order (by (62))	$\mathbb{P}_1$ order (experimental)	$\mathbb{Q}_2$ order (experimental)
0.4	$1.4 - \varepsilon$	$0.4 - \varepsilon$	0.363	0.429
0.6	$1.6 - \varepsilon$	$0.6 - \varepsilon$	0.574	0.651
1.4	$2.4 - \varepsilon$	1 for $\mathbb{P}_1$, $1.4 - \varepsilon$ for $\mathbb{Q}_2$	0.955	1.394
1.6	$2.6 - \varepsilon$	1 for $\mathbb{P}_1$, $1.6 - \varepsilon$ for $\mathbb{Q}_2$	0.952	1.518

medium regions, however, it would require a detailed description of the porous medium and its computational cost could be prohibitive. Under the (realistic) assumption that the Reynolds number in the porous domain is small, the Navier-Stokes equations could be therein up-scaled to a macroscopic level and replaced by the Darcy law.

Consider the case of a tangential flow of a fluid over a porous bed. This situation is known in literature also as *near parallel flows* [18], i.e. flows for which the pressure gradient is not normal to the interface and the Darcy velocity inside the porous domain is much smaller than the velocity in the fluid domain. The most widely used approach to couple the free fluid regime with the porous-medium one consists of:
- the introduction of an artificial sharp interface Γ between the Stokes (or fluid) domain Ω_s and the Darcy (or porous) domain Ω_d;
- the imposition of the mass conservation, the balance of normal forces and the Beavers-Joseph-Saffman (BJS) experimental law on Γ ([9]), see Fig. 20.

To write down the associated mathematical model, we introduce the following entities:

- the outward unit normal vectors $\mathbf{n}_k$ to $\partial\Omega_k$,
- the dynamic viscosity μ, the density ρ, the velocity $\mathbf{u}_s$ and the pressure p_s of the fluid in Ω_s,
- the Cauchy stress tensor for the fluid $\boldsymbol{\sigma}_s = \boldsymbol{\sigma}_s(\mathbf{u}_s, p_s) = -p_s\mathbf{I} + \mu(\nabla\mathbf{u}_s + (\nabla\mathbf{u}_s)^T)$,
- the Darcy velocity $\mathbf{u}_d$ and the intrinsic average pressure p_d in the porous domain, the intrinsic permeability $\boldsymbol{\kappa} = \boldsymbol{\kappa}(\mathbf{x})$ (for any $\mathbf{x} \in \Omega_d$) of the porous media,
- two given body forces $\mathbf{f}_s$ and $\mathbf{f}_d$,
- the normal unit vector $\mathbf{n}_\Gamma$ to Γ directed from Ω_s to Ω_d (then $\mathbf{n}_\Gamma = \mathbf{n}_s = -\mathbf{n}_d$ on Γ) and an orthonormal system of tangent vectors $\boldsymbol{\tau}_j$, with $j = 1, \ldots, d-1$ on Γ.

The coupled problem that we consider reads:

Stokes problem (fluid domain)

$$-\nabla \cdot \boldsymbol{\sigma}_s = \mathbf{f}_s, \quad \nabla \cdot \mathbf{u}_s = 0 \qquad \text{in } \Omega_s, \quad (73)$$

Darcy problem (porous domain)

$$\mathbf{u}_d = -\frac{\boldsymbol{\kappa}}{\mu}(\nabla p_d - \mathbf{f}_d), \quad \nabla \cdot \mathbf{u}_d = 0 \qquad \text{in } \Omega_d, \quad (74)$$

interface conditions (sharp interface)

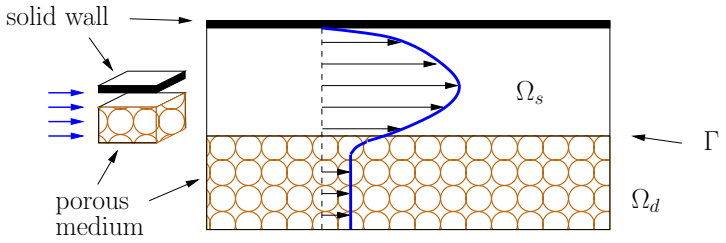

Figure 20: A typical setting of the Stokes-Darcy coupled problem for a fluid over a porous bed

$$\mathbf{u}_s \cdot \mathbf{n}_s + \mathbf{u}_d \cdot \mathbf{n}_d = 0 \qquad \text{(mass conservation)} \qquad \text{on } \Gamma, \quad (75)$$

$$(\boldsymbol{\sigma}_s \mathbf{n}_s) \cdot \mathbf{n}_s + p_d = 0 \qquad \text{(balance of normal forces)} \qquad \text{on } \Gamma, \quad (76)$$

$$(\boldsymbol{\sigma}_s \mathbf{n}_s) \cdot \boldsymbol{\tau}_j + \frac{\alpha\mu}{\sqrt{\boldsymbol{\tau}_j{}^T \boldsymbol{\kappa} \boldsymbol{\tau}_j}} \mathbf{u}_s \cdot \boldsymbol{\tau}_j = 0, \ j = 1, \ldots, d-1, \text{(BJS condition)} \qquad \text{on } \Gamma, \quad (77)$$

where α is a suitable parameter depending on the porous media. Indeed, the BJS condition is not a coupling condition, as it only involves quantities from one side. As a matter of fact, it is always used to complete the set of the boundary conditions (on the interface) for the Stokes problem in Ω_s.

The system (73)–(77) is completed with suitable boundary conditions that read (as usual, D stands for Dirichlet and N for Neumann):

$$\begin{array}{llll} \mathbf{u}_s = \mathbf{g}_s^D & \text{on } \partial\Omega_{D,s}, & \boldsymbol{\sigma}_s \mathbf{n}_s = \mathbf{0} & \text{on } \partial\Omega_{N,s}, \\ p_d = 0 & \text{on } \partial\Omega_{D,d}, & \mathbf{u}_d \cdot \mathbf{n}_d = g_d^N & \text{on } \partial\Omega_{N,d}, \end{array}$$

where we assume that $\partial\Omega_{N,k}$ and $\partial\Omega_{D,k}$ are non-intersecting subsets of $\partial\Omega_k \setminus \Gamma$ such that $\overline{\partial\Omega_{N,k} \cup \partial\Omega_{D,k}} = \overline{\partial\Omega_k \setminus \Gamma}$.

The coupled system (73)–(77) can be recast in the form (1)–(4) by associating the Stokes problem with $L_2(u_2)$ and the Darcy problem with $L_1(u_1)$.

When considering the weak (variational) formulation of the coupled problem (73)–(77), the interface coupling conditions (75) and (76) can be treated in different ways depending on the specific variational form used.

In the form used in Sect. 3.1, the balance of normal forces (76) plays the role of a Φ-like condition (2), while the mass conservation condition (75) will be treated as a Ψ-like condition (3).

In specific circumstances, however, for instance when the interface Γ is parallel to one of the cartesian coordinates, condition (75) can be easily enforced as a Dirichlet condition (thus under the form (2)) on the space of trial functions and condition (76) as a Neumann (natural) condition, e.g., like (3).

3.1 INTERNODES applied to the Stokes-Darcy system

We define the functional spaces:

$$\mathbf{V}_s = [H^1(\Omega_s)]^d, \quad \mathbf{V}_s^D = \{\mathbf{v} \in \mathbf{V}_s : \ \mathbf{v} = \mathbf{0} \text{ on } \partial\Omega_{D,s}\}, \qquad (78)$$

$$\mathbf{V}_d = \{\mathbf{v} \in [L^2(\Omega_d)]^d :\ \nabla\cdot\mathbf{v} \in L^2(\Omega_d)\}, \quad \mathbf{V}_d^N = \{\mathbf{v} \in \mathbf{V}_d :\ \mathbf{v}\cdot\mathbf{n} = 0 \text{ on } \partial\Omega_{N,d}\},$$
$$Q_s = L^2(\Omega_s), \quad Q_d = L^2(\Omega_d),$$
$$\Lambda = \{\lambda \in H^{1/2}(\Gamma) :\ \exists v \in H^1(\Omega_d),\ v = 0 \text{ on } \partial\Omega_{D,d},\ s.t.\ v_{|\Gamma} = \lambda\}. \tag{79}$$

Then we consider the following weak form of the Stokes-Darcy coupled problem (73)–(77) ([17]): find $\mathbf{u}_s \in \mathbf{V}_s$, $p_s \in Q_s$, $\mathbf{u}_d \in \mathbf{V}_d$, $p_d \in Q_d$, and $\lambda \in \Lambda$ with $\mathbf{u}_s = \mathbf{g}_s^D$ on $\partial\Omega_{D,s}$, $\mathbf{u}_d\cdot\mathbf{n}_d = g_d^N$ on $\partial\Omega_{N,d}$ such that:

$$\begin{cases} 2\mu\displaystyle\int_{\Omega_s} D(\mathbf{u}_s) : D(\mathbf{v}_s)\,d\Omega - \int_{\Omega_s} p_s\nabla\cdot\mathbf{v}_s\,d\Omega + \int_\Gamma \lambda\mathbf{v}_s\cdot\mathbf{n}_s\,d\Gamma \\ \quad + \displaystyle\sum_{j=1}^{d-1}\int_\Gamma \alpha_j(\mathbf{u}_s\cdot\boldsymbol{\tau}_j)(\mathbf{v}_s\cdot\boldsymbol{\tau}_j)\,d\Gamma = \int_{\Omega_s}\mathbf{f}_s\cdot\mathbf{v}_s\,d\Omega & \forall\mathbf{v}_s \in \mathbf{V}_s^D, \\ \displaystyle\int_{\Omega_s} q_s\nabla\cdot\mathbf{u}_s\,d\Omega = 0 & \forall q_s \in Q_s, \end{cases} \tag{80}$$

$$\begin{cases} \mu\displaystyle\int_{\Omega_d}(\boldsymbol{\kappa}^{-1}\mathbf{u}_d)\cdot\mathbf{v}_d\,d\Omega - \int_{\Omega_d} p_d\nabla\cdot\mathbf{v}_d\,d\Omega + \int_\Gamma \lambda\mathbf{v}_d\cdot\mathbf{n}_d\,d\Gamma \\ \quad = \displaystyle\int_{\Omega_d}\mathbf{f}_d\cdot\mathbf{v}_d\,d\Omega & \forall\mathbf{v}_d \in \mathbf{V}_d^N, \\ \displaystyle\int_{\Omega_d} q_d\nabla\cdot\mathbf{u}_d\,d\Omega = 0 & \forall q_d \in Q_d, \end{cases} \tag{81}$$

$$\int_\Gamma \mathbf{u}_s\cdot\mathbf{n}_s\eta + \int_\Gamma \mathbf{u}_d\cdot\mathbf{n}_d\eta = 0 \qquad \forall\eta \in \Lambda, \tag{82}$$

where $D(\mathbf{v}) = (\nabla\mathbf{v} + (\nabla\mathbf{v})^T)/2$, while $\alpha_j = \alpha\mu/\sqrt{\boldsymbol{\tau}_j^T\boldsymbol{\kappa}\boldsymbol{\tau}_j}$.

The Lagrange multiplier $\lambda \in \Lambda$ is in fact $\lambda = p_d = -(\sigma_s\mathbf{n}_s)\cdot\mathbf{n}_s$ on Γ.

We discretize both Stokes problem (73) and Darcy problem (74) by inf-sup stable (or stabilized) couples of finite elements (see, e.g., [8, 13, 19]).

Independent finite element space discretizations (as described in Sect. 2.2) are considered in Ω_s and Ω_d; moreover they may induce two different discrete interfaces $\Gamma_s = \mathcal{T}_{s,h_s} \cap \Gamma$ and $\Gamma_d = \mathcal{T}_{d,h_d} \cap \Gamma$ in the case of a curved interface Γ, see e.g. Fig. 4, right, for an example.

Then we use the subindices h_k (for $k = s, d$) to characterize the subspaces of the functional spaces (78) as well as the discrete counterpart of each variable appearing in the system (80)–(82). Then, for $k = s, d$, we consider the trace spaces Y_{k,h_k} and Λ_{k,h_k} defined as in Sect. 2.2.

In order to apply the INTERNODES method to the discrete counterpart of (80)–(82), we define the scalar quantities:

$$(r_u^{(k)})_i = \int_{\Gamma_k}(\mathbf{u}_{k,h_k}\cdot\mathbf{n}_k)\mu_i^{(k)}, \qquad i = 1,\dots,\overline{n}_k,\ k = s, d, \tag{83}$$

(where we recall that $\{\mu_i^{(k)}\}_{i=1}^{\overline{n}_k}$ are the Lagrange basis functions of Y_{k,h_k}) and

$$(z_u^{(k)})_j = \sum_{i=1}^{\overline{n}_k}(M_{\Gamma_k}^{-1})_{ji}(r_u^{(k)})_i \qquad j = 1,\dots,\overline{n}_k,\ k = s, d, \tag{84}$$

(as in Sect. 2.2, M_{Γ_k} denotes the mass matrix on the interface Γ_k) and the discrete functions (belonging to Y_{k,h_k})

$$(r_u)_{k,h_k} = \sum_{j=1}^{\overline{n}_k} (z_u^{(k)})_j \mu_j^{(k)} \tag{85}$$

that represent an approximation of the functionals $\mathbf{u}_k \cdot \mathbf{n}_k$ on Γ_k.

Moreover we consider two different discretization of the Lagrange multiplier λ: λ_{s,h_s} for the Stokes problem and λ_{d,h_d} for the Darcy one.

The INTERNODES form of problem (80)–(82) reads: find

$$\begin{array}{lll} \mathbf{u}_{s,h_s} \in \mathbf{V}_{s,h_s}, & p_{s,h_s} \in Q_{s,h_s}, & \lambda_{s,h_s} \in \Lambda_{s,h_s}, \\ \mathbf{u}_{d,h_d} \in \mathbf{V}_{d,h_d}, & p_{d,h_d} \in Q_{d,h_d}, & \lambda_{d,h_d} \in \Lambda_{d,h_d}, \end{array}$$

(satisfying the given boundary conditions) such that:

$$\left\{ \begin{array}{l} 2\mu \displaystyle\int_{\Omega_s} D(\mathbf{u}_{s,h_s}) : D(\mathbf{v}_{s,h_s})\, d\Omega - \int_{\Omega_s} p_{s,h_s} \nabla \cdot \mathbf{v}_{s,h_s}\, d\Omega + \int_{\Gamma_s} \lambda_{s,h_s} \mathbf{v}_{s,h_s} \cdot \mathbf{n}_s\, d\Gamma \\ \quad + \displaystyle\sum_{j=1}^{d-1} \int_{\Gamma_s} \alpha_j (\mathbf{u}_{s,h_s} \cdot \boldsymbol{\tau}_j)(\mathbf{v}_{s,h_s} \cdot \boldsymbol{\tau}_j)\, d\Gamma = \int_{\Omega_s} \mathbf{f}_s \cdot \mathbf{v}_{s,h_s}\, d\Omega \qquad \forall \mathbf{v}_{s,h_s} \in \mathbf{V}_{s,h_s}^D, \\ \displaystyle\int_{\Omega_s} q_{s,h_s} \nabla \cdot \mathbf{u}_{s,h_s}\, d\Omega = 0 \qquad \forall q_{s,h_s} \in Q_{s,h_s}, \end{array} \right. \tag{86}$$

$$\left\{ \begin{array}{l} \mu \displaystyle\int_{\Omega_d} (\boldsymbol{\kappa}^{-1} \mathbf{u}_{d,h_d}) \cdot \mathbf{v}_{d,h_d}\, d\Omega - \int_{\Omega_d} p_{d,h_d} \nabla \cdot \mathbf{v}_{d,h_d}\, d\Omega \\ \quad + \displaystyle\int_{\Gamma_d} \lambda_{d,h_d} \mathbf{v}_{d,h_d} \cdot \mathbf{n}_d\, d\Gamma = \int_{\Omega_d} \mathbf{f}_d \cdot \mathbf{v}_{d,h_d}\, d\Omega \qquad \forall \mathbf{v}_{d,h_d} \in \mathbf{V}_{d,h_d}^N, \\ \displaystyle\int_{\Omega_d} q_{d,h_d} \nabla \cdot \mathbf{u}_{d,h_d}\, d\Omega = 0 \qquad \forall q_{d,h_d} \in Q_{d,h_d}, \end{array} \right. \tag{87}$$

$$\begin{array}{ll} (r_u)_{d,h_d} + \Pi_{ds} (r_u)_{s,h_s} = 0 & \text{on } \Gamma_d, \\ \lambda_{s,h_s} = \Pi_{sd} \lambda_{d,h_d} & \text{on } \Gamma_s. \end{array} \tag{88}$$

The conditions (88) are the INTERNODES counterpart of the interface condition (75)–(76), obtained by applying the intergrid (interpolation) operators Π_{12} and Π_{21} defined in Sect. 2.2.

More precisely, if we make the associations $d \leftrightarrow 1$ and $s \leftrightarrow 2$, the operator $\Pi_{sd} (= \Pi_{21})$ is used to interpolate on Γ_s the discrete trace of p_{d,h_d} that is known on Γ_d, in order to provide the normal component of the Cauchy stress for the Stokes problem on the interface Γ_s. On the contrary, $\Pi_{ds} (= \Pi_{12})$ is used to interpolate on Γ_d the weak counterpart of $\mathbf{u}_{s,h_s} \cdot \mathbf{n}_s$ that is known on Γ_s, in order to provide the normal component of the Darcy velocity on the interface Γ_d.

The algebraic form of the INTERNODES conditions (88) is very similar to that written for the elliptic problem in Sect. 2.4, i.e. formulas (53) and (55). More precisely, let us denote by R_{ds} (R_{sd}, resp.) the matrix associated with the interpolation operator Π_{ds} (Π_{sd}, resp.), by $\mathbf{r}_{\overline{\Gamma}_k}$ the array whose entries are the real values $(r_u^{(k)})_i$ for $i =$

$1, \ldots, \overline{n}_k$ defined in (83) and by $\boldsymbol{\lambda}_{\overline{\Gamma}_k}$ the array whose entries are the nodal values of λ_{k,h_k} at the nodes $\mathbf{x}_i^{(\Gamma_k)}$ for $i = 1, \ldots, \overline{n}_k$.

The algebraic form of the INTERNODES conditions (88) reads:

$$\begin{aligned} &\mathbf{r}_{\overline{\Gamma}_d} + Q_{ds}\mathbf{r}_{\overline{\Gamma}_s} = \mathbf{0}, \\ &\boldsymbol{\lambda}_{\overline{\Gamma}_s} = Q_{sd}\boldsymbol{\lambda}_{\overline{\Gamma}_d} \end{aligned} \tag{89}$$

with $Q_{ds} = M_{\Gamma_d} R_{ds} M_{\Gamma_s}^{-1}$ and $Q_{sd} = R_{sd}$. In the following we consider also the matrices $Q_{ds}^0 = Q_{ds}(\mathcal{I}_{\Gamma_d}, \mathcal{I}_{\overline{\Gamma}_s})$ and $Q_{sd}^0 = Q_{sd}(\mathcal{I}_{\Gamma_d}, \mathcal{I}_{\Gamma_s})$ (see (47)).

To compute the INTERNODES solution of system (86)–(88) we can follow Algorithm 5, by which we solve the Schur complement system

$$S\boldsymbol{\lambda}_{\Gamma_d} = \mathbf{b}$$

obtained by eliminating the degrees of freedom of u_{k,h_k} and p_{k,h_k} from system (86)–(88) as we done in Sect. 2.4.1 for elliptic problems. Notice that, when non-homogeneous boundary conditions are assigned for p_d on $\partial\Omega_{D,d}$, Algorithms 5 and 6 must take into account the lifting of the boundary datum, as done for the elliptic problem in Sec. 2.4.1.

Algorithm 5 INTERNODES algorithm for Stokes-Darcy coupling

Build the intergrid matrices Q_{sd} and Q_{ds};
set $\lambda_{d,h_d} = 0$, $\lambda_{s,h_s} = 0$;
solve problems (86) and (87);
for all $k = s, d$ **do**
  compute the residuals $(r_u^{(k)})_i$ for $i = 1, \ldots, \overline{n}_k$ (see (83)) and store them in $\mathbf{r}_{\overline{\Gamma}_k}$;
end for
compute $\mathbf{b} = -(\mathbf{r}_{\Gamma_d} + Q_{ds}^0 \mathbf{r}_{\overline{\Gamma}_s})$;
solve $S\boldsymbol{\lambda}_{\Gamma_d} = \mathbf{b}$ by an iterative matrix-free method, (see Algorithm 6 for the computation of $\mathbf{v} = S\mathbf{t}_{\Gamma_d}$, for a given $\mathbf{t}_{\Gamma_d}$);
compute $\boldsymbol{\lambda}_{\Gamma_s} = Q_{sd}^0 \boldsymbol{\lambda}_{\Gamma_d}$;
set up λ_{d,h_d} and λ_{s,h_s} starting from $\boldsymbol{\lambda}_{\Gamma_d}$ and $\boldsymbol{\lambda}_{\Gamma_s}$;
solve problems (86) and (87);

3.2 Numerical results for the Stokes-Darcy coupling

We test the accuracy of INTERNODES by solving problem (73)–(77) with: $\Omega_s = (0,1) \times (1,2)$, $\Omega_d = (0,1) \times (0,1)$, $\mu = 1$, $\kappa = 10^{-2}$, $\boldsymbol{\kappa} = \kappa I$. The boundary data and the right hand side $\mathbf{f}_s = \mathbf{f}_d$ are such that the exact solution is

$$\begin{aligned} &\mathbf{u}_s = \kappa \begin{bmatrix} -\sin(\frac{\pi}{2}x)\cos(\frac{\pi}{2}y) - y + 1, \\ \cos(\frac{\pi}{2}x)\sin(\frac{\pi}{2}y) - 1 + x \end{bmatrix}, \quad p_s = 1 - x, \\ &\mathbf{u}_d = \kappa \begin{bmatrix} \sin(\frac{\pi}{2}x)\cos(\frac{\pi}{2}y) + y, \\ \cos(\frac{\pi}{2}x)\sin(\frac{\pi}{2}y) - 1 + x \end{bmatrix}, \qquad p_d = \tfrac{2}{\pi}\cos(\tfrac{\pi}{2}x)\sin(\tfrac{\pi}{2}y) - y(x-1). \end{aligned}$$

Algorithm 6 Evaluation of $\mathbf{v} = S\mathbf{t}_{\Gamma_d}$, for a given $\mathbf{t}_{\Gamma_d}$ whose entries are the dof of a discrete function that is null on $\partial\Gamma_d$. Stokes-Darcy coupling

Input: $\mathbf{t}_{\Gamma_d} \in \mathbb{R}^{n_d}$
Output: $\mathbf{v} \in \mathbb{R}^{n_d}$ s.t. $\mathbf{v} = S\mathbf{t}_{\Gamma_d}$
compute $\mathbf{t}_{\Gamma_s} = Q^0_{sd}\mathbf{t}_{\Gamma_d}$;
set up the functions t_{d,h_d} null at $\partial\Gamma_d$ and t_{s,h_s} null at $\partial\Gamma_s$ starting from $\mathbf{t}_{\Gamma_d}$ and $\mathbf{t}_{\Gamma_s}$;
solve problem (86) with $\lambda_{d,h_d} = t_{d,h_d}$, $\mathbf{f}_d = \mathbf{0}$ and null boundary conditions;
solve problem (87) with $\lambda_{s,h_s} = t_{s,h_s}$, $\mathbf{f}_s = \mathbf{0}$ and null boundary conditions;
for all $k = s, d$ **do**
    compute the residuals $(r_u^{(k)})_i$ for $i = 1, \ldots, \overline{n}_k$ (see (83)) and store them in $\mathbf{r}_{\overline{\Gamma}_k}$;
end for
compute $\mathbf{v} = -(\mathbf{r}_{\Gamma_d} + Q^0_{ds}\mathbf{r}_{\overline{\Gamma}_s})$;

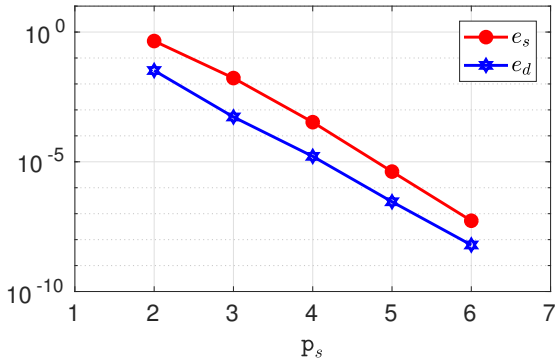

Figure 21: The errors versus the polynomial degree for the Stokes-Darcy problem (73)–(77) solved on non-conforming meshes by the INTERNODES method, with mesh-sizes $h_s = 1/5$, $h_d = 1/3$, and polynomial degrees $\mathtt{p}_d = \mathtt{p}_s + 1$

In both the subdomains we consider stabilized SEM (see [13] for the Stokes problem and [19, 8] for the Darcy one).

The errors

$$e_s = \frac{\|\mathbf{u}_s - \mathbf{u}_{s,h_s}\|_{H^1(\Omega_s)}}{\|\mathbf{u}_s\|_{H^1(\Omega_s)}} + \frac{\|p_s - p_{s,h_s}\|_{L^2(\Omega_s)}}{\|p_s\|_{L^2(\Omega_s)}},$$
$$e_d = \frac{\|\mathbf{u}_d - \mathbf{u}_{d,h_d}\|_{L^2(\Omega_d)}}{\|\mathbf{u}_d\|_{L^2(\Omega_d)}} + \frac{\|p_d - p_{d,h_d}\|_{H^1(\Omega_d)}}{\|p_d\|_{H^1(\Omega_d)}}$$

are shown in Figures 21 and 22. The local polynomial degrees of the *hp*-fem discretizations are denoted by $\mathtt{p}_s$ and $\mathtt{p}_d$.

We observe that the errors decay exponentially w.r.t. the polynomial degrees (Fig. 21), and with order $q = \mathtt{p}_s = \mathtt{p}_d$ w.r.t. the mesh sizes (Fig. 22), as for the approximation of elliptic problems.

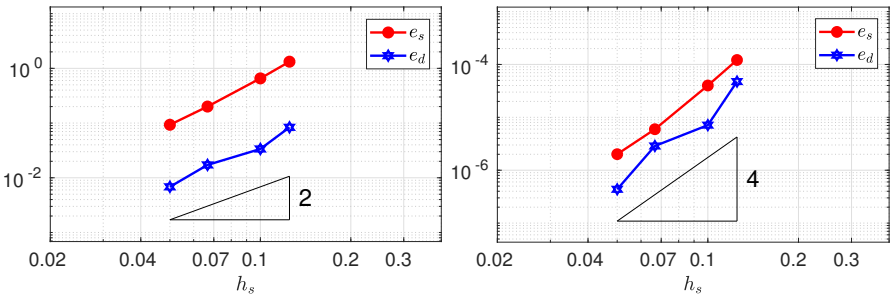

Figure 22: The errors versus the mesh size h_s for the Stokes-Darcy problem (73)–(77) solved on non-conforming meshes by the INTERNODES method. The following couples for the mesh sizes are considered: $h_s = 1/8$ and $h_d = 1/5$, $h_s = 1/10$ and $h_d = 1/8$, $h_s = 1/15$ and $h_d = 1/10$, $h_s = 1/20$ and $h_d = 1/16$. The polynomial degrees are $\mathtt{p}_s = \mathtt{p}_d = 2$ (at left) and $\mathtt{p}_s = \mathtt{p}_d = 4$ (at right)

3.3 The cross-flow membrane filtration test case

In Fig. 24 we show the INTERNODES solution computed for the *cross-flow membrane filtration* test case with non-flat interface Γ. The data for this test case are inspired from [16] (see also [8]). The domain is $\Omega = (0, 0.015) \times (-0.0075, 0)$ (in meters). The coordinates (x, z) are used. The domain Ω_s represents a part of channel closed on the top side where the fluid can flow through the vertical sides, while Ω_d represents a vertical filter. The fluid is water, the porous medium will be characterized by its isotropic intrinsic permeability $\boldsymbol{\kappa} = \kappa \mathbf{I}$. The interface Γ is a piece-wise linear function (see Fig. 23, left).

We suppose that the fluid is subject to the gravitational force, thus $\mathbf{f}_1 = \mathbf{f}_2 = (0, -\rho g)^t$ $[kg/(m^2\, s^2)]$, where ρ is the density of the water and g the gravity acceleration. The fluid enters into the domain Ω_s through the vertical left-hand boundary, where we impose a parabolic inflow $\mathbf{u}_s = \mathbf{g}_s = (-16 \cdot 10^3 z(z + 0.005), 0)^t$, on the top side of the domain Ω_s we set the no-slip boundary conditions $\mathbf{u}_s = \mathbf{0}$, while the fluid may leave the domain through the vertical right-hand boundary $\boldsymbol{\sigma}_s \cdot \mathbf{n}_s = 9.8\rho z \mathbf{n}_s$. Concerning the boundary conditions for the porous domain, we impose $\mathbf{u}_d \cdot \mathbf{n}_d = 0$ on the vertical sides to mimic the presence of an impervious material outside the domain, while we set $p_d = -\rho g z$ on the bottom horizontal side to account for the presence of a stationary fluid below the porous domain. The amount of flux filtering through the interface depends on the permeability of the porous media and on the boundary data imposed on the bottom horizontal side on the pressure.

As in the previous test case, stabilized SEM have been used for the discretization in either Ω_s and Ω_d. In Fig. 23, right, we plot the non-conforming meshes used in the simulation, corresponding to 48 quads with $p_s = 6$ in Ω_s and 24 quads with $p_d = 3$ in Ω_d.

In Fig. 24 we show the INTERNODES solution corresponding to the permeability $\kappa = 10^{-7}$: at left the velocity field, at right the hydrodynamic pressure, i.e. the function p_{hyd} such that $p_{hyd}|_{\Omega_k} = p_k + \rho g z$ for $k = s, d$.

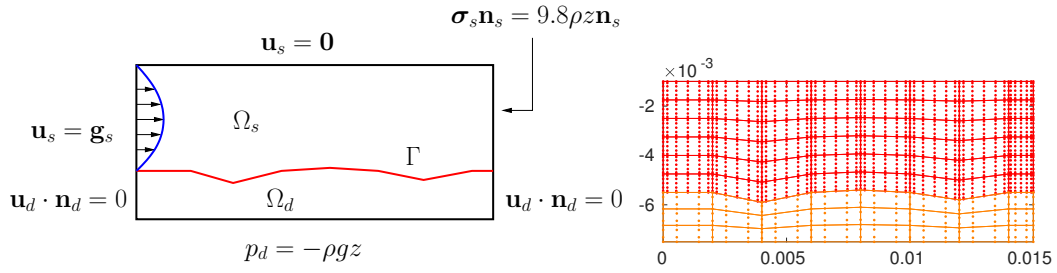

Figure 23: The geometry and the mesh used in the cross-flow membrane filtration test case

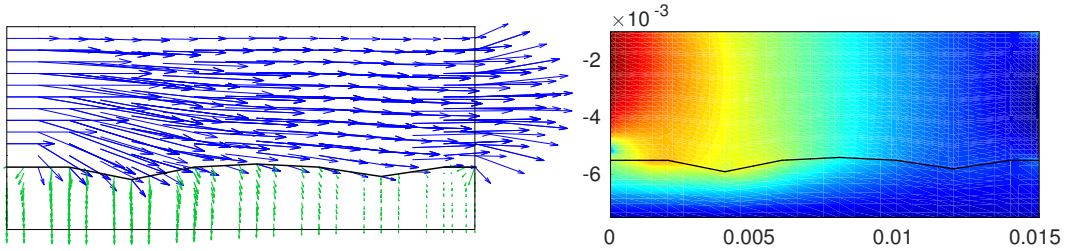

Figure 24: INTERNODES solution of the Stokes-Darcy coupling for the cross-flow membrane filtration test case, with $\kappa = 10^{-7}$. At left, the velocity field, at right the hydrodynamic pressure

Numerical results show that INTERNODES maintaines the optimal accuracy of the local discretizations and that it is a versatile method to deal with non-conforming interfaces.

References

[1] C. Bègue, C. Bernardi, N. Debit, Y. Maday, G.E. Karniadakis, C. Mavriplis, and A.T. Patera. Nonconforming spectral element-finite element approximations for partial differential equations. In *Proceedings of the Eighth International Conference on Computing Methods in Applied Sciences and Engineering (Versailles, 1987)*, volume 75, pages 109–125, 1989.

[2] C. Bernardi, Y. Maday, and A.T. Patera. A new nonconforming approach to domain decomposition: the mortar element method. In *Nonlinear partial differential equations and their applications. Collège de France Seminar, Vol. XI (Paris, 1989–1991)*, volume 299 of *Pitman Res. Notes Math. Ser.*, pages 13–51. Longman Sci. Tech., Harlow, 1994.

[3] H. J. Brauchli and J. T. Oden. Conjugate approximation functions in finite-element analysis. *Quart. Appl. Math.*, 29:65–90, 1971.

[4] R. Dautray and J.-L. Lions. *Mathematical analysis and numerical methods for science and technology*, volume 2. Springer, Berlin, 2000.

[5] S. Deparis, D. Forti, P. Gervasio, and A. Quarteroni. INTERNODES: an accurate interpolation-based method for coupling the Galerkin solutions of PDEs on subdomains featuring non-conforming interfaces. *Computers & Fluids*, 141:22–41, 2016.

[6] S. Deparis, D. Forti, and A. Quarteroni. A rescaled localized radial basis function interpolation on non-Cartesian and nonconforming grids. *SIAM J. Sci. Comput.*, 36(6):A2745–A2762, 2014.

[7] S. Deparis, D. Forti, and A. Quarteroni. *A fluid-structure interaction algorithm using radial basis function interpolation between non-conforming interfaces*, pages 439–450. Modeling and Simulation in Science, Engineering and Technology. Springer, 2016.

[8] M. Discacciati, P. Gervasio, A. Giacomini, and A. Quarteroni. Interface Control Domain Decomposition (ICDD) Method for Stokes-Darcy coupling. *SIAM J. Numer. Anal.*, 54(2):1039–1068, 2016.

[9] M. Discacciati and A. Quarteroni. Navier-Stokes/Darcy coupling: modeling, analysis, and numerical approximation. *Rev. Mat. Complut.*, 22(2):315–426, 2009.

[10] D. Forti. *Parallel Algorithms for the Solution of Large-Scale Fluid-Structure Interaction Problems in Hemodynamics*. PhD thesis, École Polytechnique Fédérale de Lausanne, Lausanne (Switzerland), 4 2016.

[11] P. Gervasio and A. Quarteroni. Analysis of the INTERNODES method for non-conforming discretizations of elliptic equations. *Comput. Methods Appl. Mech. Engrg.*, 334:138–166, 2018.

[12] P. Gervasio and A. Quarteroni. Internodes for heterogeneous couplings. In *Domain decomposition methods in science and engineering XXIV*, volume 125 of *Lect. Notes Comput. Sci. Eng.*, pages 61–73. Springer International Publishing, 2018. (in press).

[13] P. Gervasio and F. Saleri. Stabilized spectral element approximation for the Navier-Stokes equations. *Numerical Methods for Partial Differential Equations*, 14:115–141, 1998.

[14] P. Grisvard. *Elliptic Problems in Nonsmooth Domains*. Pitman (Advanced Publishing Program), Boston, MA, 1985.

[15] V. Gupta, C.A. Duarte, I. Babuška, and U. Banerjee. Stable GFEM (SGFEM): improved conditioning and accuracy of GFEM/XFEM for three-dimensional fracture mechanics. *Comput. Methods Appl. Mech. Engrg.*, 289:355–386, 2015.

[16] N.S. Hanspal, A.N. Waghode, V. Nassehi, and R.J. Wakeman. Development of a predictive mathematical model for coupled Stokes/Darcy flows in cross-flow membrane filtration. *Chem. Eng. J.*, 149:132–142, 2009.

[17] W.J. Layton, F. Schieweck, and I. Yotov. Coupling fluid flow with porous media flow. *SIAM J. Numer. Anal.*, 40(6):2195–2218 (2003), 2002.

[18] T. Levy and E. Sánchez-Palencia. On boundary conditions for fluid flow in porous media. *Internat. J. Engrg. Sci.*, 13(11):923–940, 1975.

[19] A. Masud and T.J.R. Hughes. A stabilized mixed finite element method for Darcy flow. *Comput. Methods Appl. Mech. Engrg.*, 191(39-40):4341–4370, 2002.

[20] P. Morin, R.H. Nochetto, and K.G. Siebert. Data oscillation and convergence of adaptive FEM. *SIAM J. Numer. Anal.*, 38(2):466–488 (electronic), 2000.

[21] A. Quarteroni. *Numerical Models for Differential Problems, 2nd ed.* Springer, 2014.

[22] A. Quarteroni and A. Valli. *Numerical Approximation of Partial Differential Equations*. Springer Verlag, Heidelberg, 1994.

[23] A. Quarteroni and A. Valli. *Domain Decomposition Methods for Partial Differential Equations*. Oxford University Press, 1999.

[24] A. Toselli and O. Widlund. *Domain decomposition methods—algorithms and theory*, volume 34 of *Springer Series in Computational Mathematics*. Springer-Verlag, Berlin, 2005.

[25] H. Wendland. Piecewise polynomial, positive definite and compactly supported radial functions of minimal degree. *Advances in computational Mathematics*, 4(1):389–396, 1995.

MOX Technical Reports, last issues

Dipartimento di Matematica
Politecnico di Milano, Via Bonardi 9 - 20133 Milano (Italy)

47/2018 Stefanucci, M.; Sangalli, L.M.; Brutti, P.
PCA-based discrimination of partially observed functional data, with an application to Aneurisk65 dataset

48/2018 Arnone, E.; Azzimonti, L.; Nobile, F.; Sangalli, L.M.
Modeling spatially dependent functional data via regression with di fferential regularization

49/2018 Massi, M.C.; Ieva, F.; Lettieri, E.
Data Mining Application to Healthcare Fraud Detection: A Two-Step Unsupervised Clustering Model for Outlier Detection with Administrative Databases

46/2018 Riccobelli, D.; Ciarletta, P.
Morpho-elastic model of the tortuous tumour vessels

45/2018 Bernardi, M.S.; Carey, M.; Ramsay, J.O.; Sangalli, L.M.
Modeling spatial anisotropy via regression with partial di fferential regularization

44/2018 Bernardi, M.S.; Sangalli, L.M.
Modelling spatially dependent functional data by spatial regression with differential regularization

43/2018 Fontana, L.; Masci, C.; Ieva, F.; Paganoni, A.M.
Performing Learning Analytics via Generalized Mixed-Effects Trees

42/2018 Antonietti, P.F.; Melas, L.
Algebraic multigrid schemes for high-order discontinuous Galerkin methods

41/2018 Mazzieri, I.; Melas, L.; Smerzini, C.; Stupazzini, M.
The role of near-field ground motion on seismic risk assessment in large urban areas

39/2018 Ferro, N.; Micheletti, S.; Perotto, S.
Density-based inverse homogenization with anisotropically adapted elements